Molecular Therapy
Original Article

Immunosuppressant therapy averts rejection of allogeneic *FKBP1A*-disrupted CAR-T cells

Colby R. Maldini,[1] Angelica C. Messana,[1] Paula B. Bendet,[1] Adam J. Camblin,[1] Faith M. Musenge,[1] Moriah L. White,[1] Joseph J. Rocha,[1] Lindsey J. Coholan,[1] Cisem Karaca,[1] Frederick Li,[1] Bo Yan,[1] Vladimir D. Vrbanac,[3] Emily Marte,[2] Daniel T. Claiborne,[2,4] Christian L. Boutwell,[2] and Todd M. Allen[2,5]

[1]Beam Therapeutics, Cambridge, MA 02142, USA; [2]Ragon Institute of Mass General, MIT and Harvard, Cambridge, MA 02139, USA; [3]Hummanized Immune System Mouse Program, Ragon Institute of Mass General, MIT and Harvard, Cambridge, MA 02139, USA; [4]Vaccine and Immunotherapy Center, The Wistar Institute, Philadelphia, PA 19104, USA; [5]Department of Medicine, Massachusetts General Hospital, Boston, MA 02115, USA

Chimeric antigen receptor (CAR) T cells from allogeneic donors promise "off-the-shelf" availability by overcoming challenges associated with autologous cell manufacturing. However, recipient immunologic rejection of allogeneic CAR-T cells may decrease their *in vivo* lifespan and limit treatment efficacy. Here, we demonstrate that the immunosuppressants rapamycin and tacrolimus effectively mitigate allorejection of HLA-mismatched CAR-T cells in immunocompetent humanized mice, extending their *in vivo* persistence to that of syngeneic humanized mouse-derived CAR-T cells. In turn, genetic knockout (KO) of FKBP prolyl isomerase 1A (*FKBP1A*), which encodes a protein targeted by both drugs, was necessary to confer CD19-specific CAR-T cells (19CAR) robust functional resistance to these immunosuppressants. *FKBP1A*^{KO} 19CAR-T cells maintained potent *in vitro* functional profiles and controlled *in vivo* tumor progression similarly to untreated 19CAR-T cells. Moreover, immunosuppressant treatment averted *in vivo* allorejection permitting *FKBP1A*^{KO} 19CAR-T cell-driven B cell aplasia. Thus, we demonstrate that genome engineering enables immunosuppressant treatment to improve the therapeutic potential of universal donor-derived CAR-T cells.

INTRODUCTION

Allogeneic chimeric antigen receptor (CAR) T cell therapies promise to deliver breakthroughs in the treatment of cancer. The development of universal donor-derived CAR-T cells could provide "off-the-shelf" availability, which simplifies patient delivery, reduces wait time to treatment, and eliminates manufacturing failure inherent to autologous cell therapies.[1–3] Despite these advantages, HLA mismatch between allogeneic donor and recipient patients may represent a barrier that limits the efficacy of allogeneic CAR-T cell therapy. Inactivation of the T cell receptor (TCR) in allogeneic CAR-T cells can prevent graft-versus-host disease (GVHD),[4–6] but the expression of mismatched HLA alleles renders allogeneic cells susceptible to recipient T cell-mediated rejection.[7] Notably, although genetic disruption of β-2-microglobulin (*B2M*) and class II transcriptional activator (*CIITA*) effectively ablate HLA surface expression and abrogate recognition by recipient T cells,[8,9] HLA class I-deficient cells are now susceptible to missing self-recognition and lysis by NK cells.[10] Thus, HLA surface expression on allogeneic CAR-T cells represents a quandary necessitating alternative immune-modulatory strategies to overcome rejection.

Immunosuppressants are routinely used in transplant medicine to mitigate the intensity of an immune reaction. For example, immunosuppressants may condition the recipient to accept a transplanted organ from an unrelated donor[11,12] and similarly limit GVHD-induced organ tissue damage from transplanted allogeneic hematopoietic stem cells.[13,14] Two common immunosuppressants, rapamycin (RPM) and tacrolimus (TAC), are structural analogs both of which bind the immunophilin FKBP prolyl isomerase 1A (FKBP1A).[15] However, these drugs differentially regulate immune responses either by inhibiting mTOR[16–18] or calcineurin-induced NFAT activation,[19] respectively. The downstream consequences of these drug-FKBP1A interactions attenuate immune cell proliferation, response to IL-2, and pro-inflammatory cytokine secretion.[20–23] Given that RPM and TAC bind a common intracellular protein, disruption of the gene encoding FKBP1A in allogeneic CAR-T cells may confer upon them drug resistance while simultaneously enabling immunosuppressant treatment to avert recipient allorejection of the CAR-T cells.

Here, we leveraged stringent humanized mouse models to interrogate a strategy that combines immunosuppressant treatment to inhibit alloreactivity and genome engineering to confer allogeneic CAR-T cell functional resistance to suppression. To do so, we first established that RPM and TAC treatment reduced recipient-driven immunologic rejection of HLA-mismatched CAR-T cells. Next, we demonstrated that *FKBP1A*-disrupted CD19-specific CAR-T cells maintained functional immune responses that controlled tumor progression and induced B cell aplasia *in vivo* amid immunosuppressant therapy.

Received 18 March 2024; accepted 14 June 2024;
https://doi.org/10.1016/j.ymthe.2024.06.022.

Correspondence: Colby R. Maldini, Beam Therapeutics, Cambridge, MA 02142, USA.
E-mail: cmaldini@beamtx.com

Furthermore, we confirmed that the *in vivo* persistence of allogeneic CAR-T cells required concurrent immunosuppressant treatment, whereafter drug treatment interruption the recipient immune response cleared allogeneic CAR-T cells. Together, these findings highlight an effective approach to overcome allorejection of "off-the-shelf" CAR-T cells and provides a means of controlling the duration of the CAR-T cell therapy.

RESULTS

HLA class I expression dictates susceptibility of allogeneic cells to rejection by T cells or NK cells

HLA-mismatched allogeneic cells elicit responses by the recipient immune system.[7] Thus, we obscured host T cell recognition by ablating HLA class I (HLA-I) and HLA class II (HLA-II) surface expression using base editing to knockout (KO) *B2M* and *CIITA*, respectively (Figures 1A–1C). HLA-deficient T cells were invisible to alloreactive T cells and resisted elimination in mixed leukocyte assays (Figures 1D and 1E). To confirm these findings *in vivo* we employed humanized immune system (HIS) mice that are capable of rejecting HLA-mismatched cells[24,25] (Figure S1). HIS mice were co-infused with an equal amount of HLA$^+$ and HLA-deficient ($B2M^{KO}CIITA^{KO}$) T cells from an unrelated human donor (Figure 1F). These allogeneic T cells were also base edited to disrupt TCR expression preventing GVHD (Figure S2) and engineered to express a non-targeting CD4-based CAR (4CAR) with a molecular tag facilitating *ex vivo* identification by flow cytometry (Figure S3). After transfer into HLA-mismatched HIS mice, allogeneic HLA$^+$ 4CAR-T cells were rapidly eliminated from circulation (Figures 1G and 1H) and tissue (Figure 1I), whereas HLA-deficient 4CAR-T cells persisted for the study duration (Figures 1G–1I).

Although the absence of HLA surface expression mitigated T cell-driven allorejection, we found that disruption of HLA-I, not HLA-II, sensitized allogeneic T cells to *in vitro* NK cell-mediated lysis (Figure 1J) and elicited robust NK cell degranulation (Figure 1K). Yet, HIS mice did not readily reject HLA-deficient T cells (Figure 1H) and, congruent with previous reports,[26–28] our data indicated that their NK cell compartment is underdeveloped relative to adult humans. For example, the degree of NK cell reconstitution in peripheral blood of HIS mice is markedly less than in humans (Figure S4A), and NK cells from HIS mice required priming with recombinant IL-15 protein to become functionally competent and reject HLA-I-deficient 4CAR-T cells (Figures S4B–S4E). However, repetitive IL-15 treatment of HIS mice induced systemic toxicity and weight loss, which prevented longitudinal assessment of 4CAR-T cell persistence (Figure S4F). Therefore, we assessed the fate of HLA-I-deficient 4CAR-T cells in a humanized NK cell (huNK) mouse model devoid of endogenous T cells.[29] Here, primary human CD56$^+$ NK cells were transplanted into NSG-IL-15 transgenic (tg) mice. After 2 weeks post-engraftment, allogeneic TCR^{KO} HLA$^+$ and TCR^{KO} HLA-I$^-$ ($B2M^{KO}$) 4CAR-T cells were co-infused into huNK mice and unreconstituted NSG-IL-15tg control mice (Figure 1L). In contrast to HIS mice, huNK mice rapidly rejected HLA-I$^-$ 4CAR-T cells, while HLA$^+$ 4CAR-T cells resisted elimination (Figures 1M and 1N). Together, these data support that the status of HLA-I expression on allogeneic T cells largely dictates susceptibility to either host T cell- or NK cell-mediated rejection.

Retention of HLA-I expression is necessary to broadly inhibit NK cell reactivity toward allogeneic T cells

Approaches to restore NK cell tolerance by engaging HLA-specific inhibitory receptors include forced expression of an invariant HLA single-chain (SC) molecule into $B2M^{KO}$ T cells (Figure 2A),[30–32] or targeted disruption of HLA alleles.[33,34] However, broad implementation of these strategies may be challenged by the heterogeneous expression pattern of HLA-specific inhibitory receptors governing NK cell activity[35,36] (Figure 2B). This stochastic expression yields NK cell subsets either lacking or expressing one or more inhibitory killer cell Ig-like receptors (KIRs) (Figure S5), resulting in distinct NK cells that may react toward cells without the appropriate HLA/KIR ligand(s). Indeed, during co-culture allogeneic $B2M^{KO}$ T cells expressing an HLA-Bw4^{SC}, HLA-C1^{SC}, HLA-C2^{SC}, or HLA-E^{SC} molecule attenuated degranulation by NK cells that expressed the corresponding HLA-specific inhibitory receptor either KIR3DL1, KIR2DL2/L3, KIR2DL1, or NKG2A, respectively (Figures 2C and S6). However, these HLA^{SC} molecules failed to reduce the net frequency of responding CD107a$^+$ total NK cells to levels observed by stimulation with unmodified (HLA-I$^+$) allogeneic T cells (Figure 2D). Furthermore, HLA^{SC} molecules did not substantially protect $B2M^{KO}$ T cells from lysis by NK cells unlike unmodified T cells that were not eliminated (Figure 2E). These data suggest that the overall benefit of an HLA^{SC} was nullified due to the insufficient frequency of NK cell subsets expressing the corresponding HLA-specific inhibitory receptor, whereas broad inhibition by allogeneic T cells required the full complement of HLA-I alleles.

Immunosuppression treatment mitigates *in vivo* rejection of allogeneic HLA-mismatched CAR-T cells

Given that complete retention of HLA-I surface expression was required to broadly inhibit NK cell reactivity toward allogeneic T cells, we investigated an alternative strategy where immunosuppressant treatment could be leveraged to avert rejection of HLA-mismatched CAR-T cells. We first determined if immunosuppressants prevented the *in vitro* priming of alloreactive T cells. To do so, we cultured peripheral blood mononuclear cells and CellTrace Violet (CTV)-labeled T cells from HLA-mismatched donors in the presence of RPM, TAC, or vehicle (VEH) control. As expected, the addition of immunosuppressants severely attenuated the proliferation of alloreactive CD4$^+$ and CD8$^+$ CTV-labeled T cells relative to VEH treatment (Figure S7). Next, we tested whether immunosuppressants alleviated *in vivo* rejection of allogeneic HLA-I$^+$ 4CAR-T cells. Five cohorts of HIS mice derived from unrelated human donors were injected daily with RPM, TAC, or VEH for 2 weeks, and at 1 day post-treatment initiation all mice received an equal amount of allogeneic TCR^{KO} HLA$^+$ and TCR^{KO} HLA-deficient 4CAR-T cells (Figure 3A). Syngeneic HIS mouse-derived 4CAR-T cells were also infused into mice in cohorts 3 and 4 to control for autologous cell persistence.

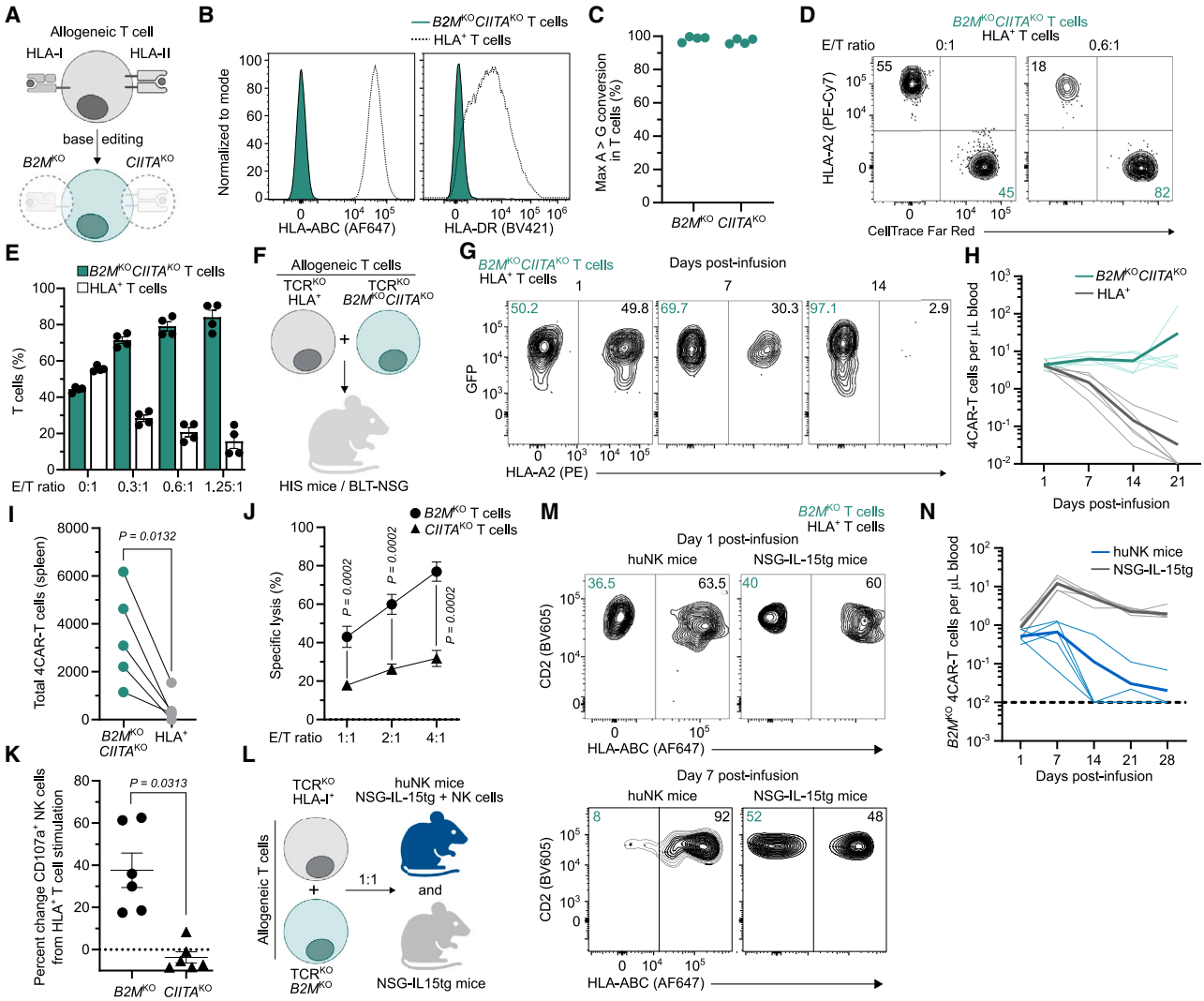

Figure 1. HLA-I expression influences susceptibility of allogeneic T cells to recipient T cell or NK cell-driven rejection

(A) Generation of allogeneic HLA-I- and HLA-II-deficient T cells using base editing to knock out (KO) *B2M* and *CIITA*, respectively. (B and C) Histograms indicate HLA-I and HLA-II surface expression (B) and frequency of on-target A>G nucleotide conversion by next-generation sequencing (C) in T cells base edited with *B2M*- and *CIITA*-specific sgRNAs and ABE8.20m mRNA. Symbols represent independent donors. (D and E) Mixed leukocyte assay as described in the materials and methods. FACS plots (D) and summarized data (E) for frequency of allogeneic $B2M^{KO}CIITA^{KO}$ and HLA^+ T cells after culture with HLA-mismatched alloreactive T cells at different effector-to-target (E/T) ratios. Symbols represent allogeneic cells from independent experiments in duplicate. (F–I) Allogeneic CD4-based CAR-T cells (4CAR) co-expressed GFP and were base edited to disrupt T cell receptor expression (TCR^{KO}), or TCR^{KO}, $B2M^{KO}$, and $CIITA^{KO}$. 4CAR-T cells (5×10^6) of each type were infused into HLA-mismatched humanized immune system (HIS) mice (BLT-NSG; $n = 6$) (F). (G and H) FACS plots indicate frequency (G) and summarized data show concentration (H) of peripheral HLA^+ and $B2M^{KO}CIITA^{KO}$ 4CAR-T cells. (I) Total 4CAR-T cells from individual mouse splenic tissue 60 days post-infusion. (J) NK cell cytotoxicity assay as described in materials and methods. Percentage specific lysis of allogeneic $B2M^{KO}$ T cells and $CIITA^{KO}$ T cells at different E/T ratios. Symbols represent mean of four independent NK cell donors in duplicate. (K) Percentage change in $CD107a^+$ NK cells after stimulation with $B2M^{KO}$ T cells or $CIITA^{KO}$ T cells from unmodified T cell control. Symbols indicate NK cells from three independent donors in duplicate. (L–N) Allogeneic TCR^{KO} and $TCR^{KO}B2M^{KO}$ 4CAR-T cells (5×10^6) were infused into huNK mice ($n = 5$) or NSG-IL-15tg mice ($n = 5$) (L). (M and N) FACS plots indicate frequency (M) and summarized data shows concentration (N) of peripheral $B2M^{KO}$ 4CAR-T cells in recipient mice. (H and N) Dotted and bold lines indicate individual mice or mean, respectively. Statistical significance was calculated by paired Student's t test (I) and Wilcoxon rank-sum test (J and K). Error bars show ±SEM, and sample sizes indicate biologically independent animals.

Both allogeneic 4CAR-T cell populations were equally detected in the peripheral blood from all groups at 1 day post-infusion but, thereafter, we observed rapid depletion of circulating HLA^+ 4CAR-T cells and persistence of HLA-deficient 4CAR-T cells in VEH-treated mice. However, RPM and TAC treatment significantly mitigated rejection of allogeneic HLA^+ 4CAR-T cells at 1 and 2 weeks post-treatment initiation (Figures 3B, 3C, and S8). We also observed that allogeneic HLA^+ 4CAR-T cells from RPM-treated mice persisted to the same

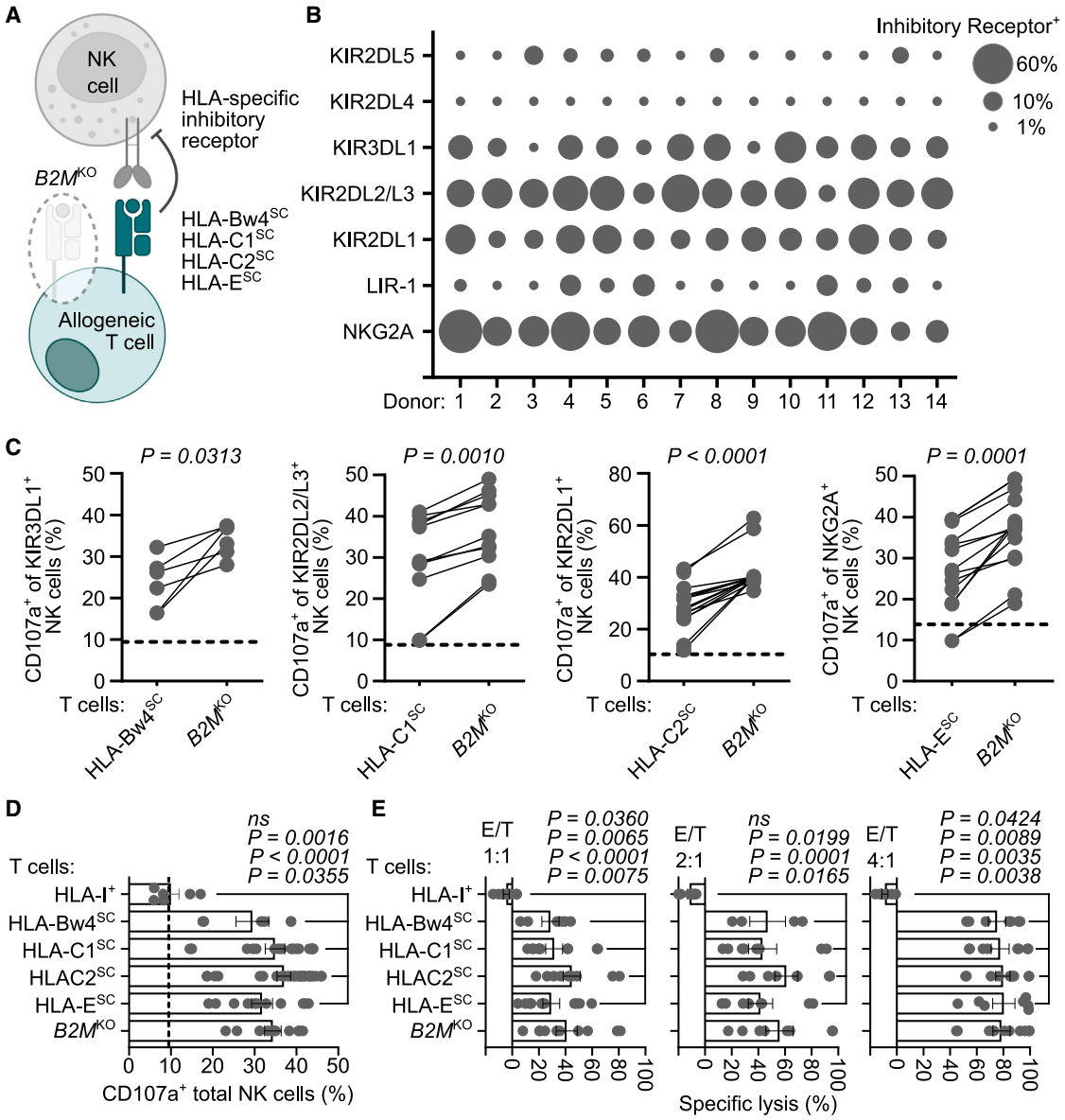

Figure 2. HLA-I retention by allogeneic T cells broadly inhibits NK cell reactivity

(A) Schematic of allogeneic HLA-I-deficient (*B2M*^{KO}) T cells expressing an HLA-I single-chain (HLA^{SC}) molecule that inhibits NK cells by engaging a cognate HLA-specific inhibitory receptor. (B) Bubble plot indicates frequency of CD56$^+$ NK cells expressing the indicated HLA-specific inhibitory receptor from 14 independent human donors. (C and D) NK cells were stimulated with allogeneic HLA-I$^+$ T cells, *B2M*^{KO} T cells, or *B2M*^{KO} T cells engineered to express one HLA^{SC}: HLA-Bw4^{SC} (HLA-B*57), HLA-C1^{SC} (HLA-C*01:02 or C*07:02), HLA-C2^{SC} (HLA-C*04:01, C*05:01, C*06:02, or C*18:01), or HLA-E^{SC} (HLA-E*01:03). (C) Summarized data indicate frequency of NK cell subsets expressing the indicated HLA-specific inhibitory receptor that were CD107a$^+$ after stimulation with allogeneic HLA-I$^+$ T cells, *B2M*^{KO} T cells, or *B2M*^{KO} T cells expressing the HLA^{SC} inhibitory ligand for the corresponding NK cell subset (i.e., KIR3DL1-HLA-Bw4^{SC}, KIR2DL2/L3-HLA-C1^{SC}, KIR2DL1-HLA-C2^{SC}, NKG2A-HLA-E^{SC}). Horizontal dashed line indicates average frequency of CD107a$^+$ NK cells after stimulation with allogeneic HLA-I$^+$ T cells. (D) Frequency of total CD107a$^+$ NK cells after stimulation with the indicated target T cell population. Vertical dashed line indicates average frequency of CD107a$^+$ NK cells in the absence of stimulation. (E) NK cell cytotoxicity assay as described in materials and methods. Percentage specific lysis of allogeneic HLA-I$^+$ T cells, *B2M*^{KO} T cells, or *B2M*^{KO} T cells engineered to express the indicated HLA^{SC} molecule 48 h post-culture at different E/T ratios. (C–E) Symbols represent aggregated data from three to five independent NK cell donors in duplicate. Bars indicate mean and error bars show ±SEM. Statistical significance was calculated by Wilcoxon matched pairs signed rank test (C) and Kruskall-Wallace test with Dunn's test for multiple comparisons (D and E).

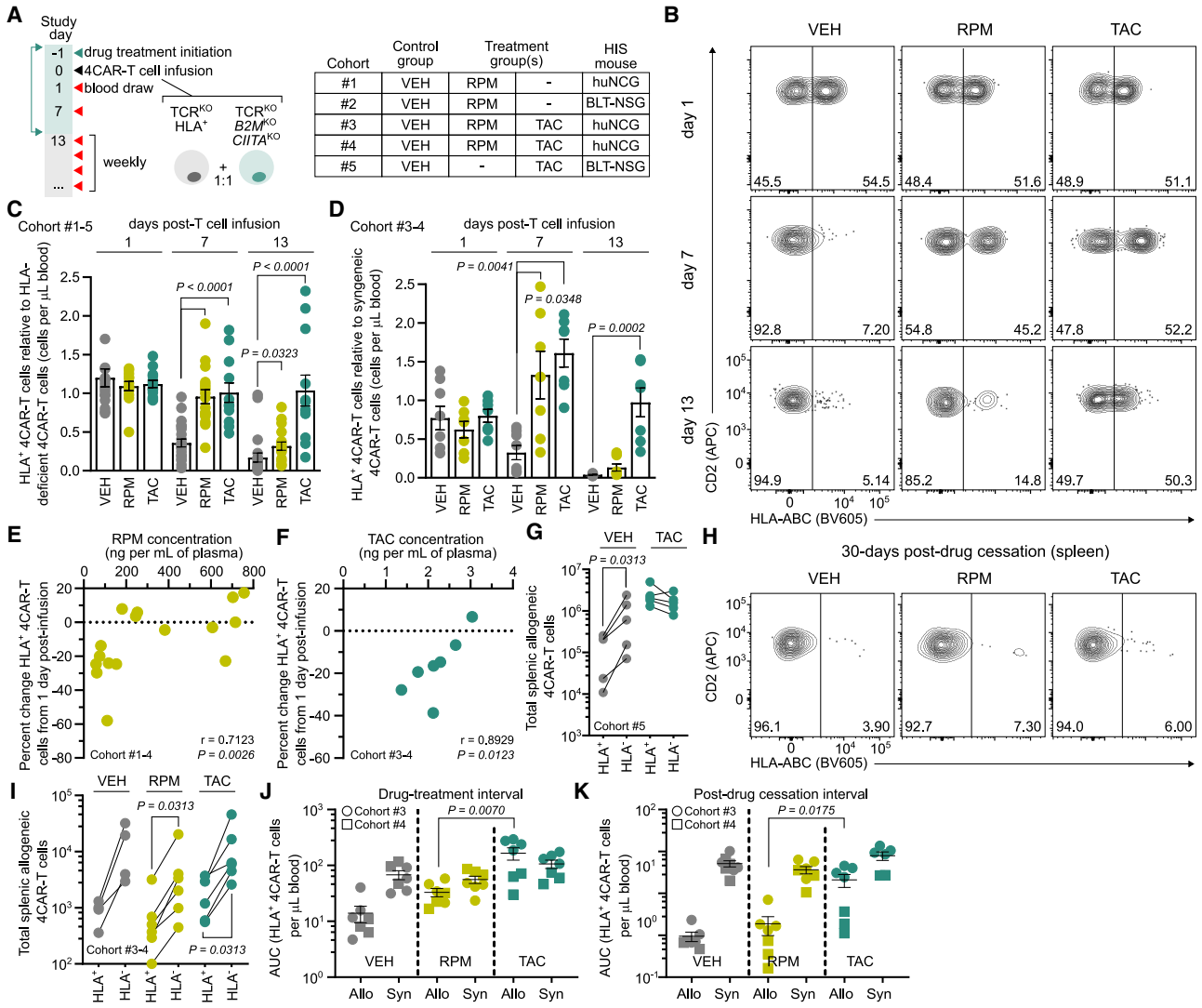

Figure 3. Immunosuppressant treatment mitigates *in vivo* rejection of allogeneic HLA-I$^+$ CAR-T cells

(A) Five HIS mouse cohorts (1–5) were allocated into groups receiving vehicle (VEH) (n = 25), rapamycin (RPM) (n = 14), or tacrolimus (TAC) (n = 13) daily for 2 weeks. At 1 day post-treatment, 5 × 10^6 allogeneic, TCR^{KO} (HLA$^+$) and TCR^{KO}*B2M*^{KO}*CIITA*^{KO} (HLA-deficient) 4CAR-T cells were mixed and infused into HLA-mismatched mice. Mice in cohorts 3 and 4 also received an equal amount of syngeneic HIS mouse-derived 4CAR-T cells. (B) FACS plots indicate longitudinal frequency of peripheral allogeneic HLA$^+$ and HLA-deficient 4CAR-T cells in VEH-, RPM-, or TAC-treated mice at 1, 7, and 13 days post-infusion. (C) Aggregate peripheral allogeneic HLA$^+$ 4CAR-T cell persistence relative to HLA-deficient 4CAR-T cells from individual mice in cohorts 1–5 during the drug treatment interval. (D) Peripheral allogeneic HLA$^+$ 4CAR-T cell persistence relative syngeneic HIS mouse-derived 4CAR-T cells from individual mice in cohorts 3–4 during the drug treatment interval. (E and F) Correlation between percentage change in allogeneic HLA$^+$ 4CAR-T cells from 1 to 7 days post-infusion and contemporaneous trough plasma concentration of RPM in cohorts 1–4 (E) and TAC in cohorts 3–4 (F) at 7 days post-infusion. (G) Total splenic allogeneic HLA$^+$ and HLA-deficient 4CAR-T cells from individual mice treated with VEH (n = 5) and TAC (n = 5) in cohort 5, 1 day post-drug withdrawal. (H and I) FACS plots indicate frequency (H) and summarized data show total (I) splenic allogeneic HLA$^+$ and HLA-deficient 4CAR-T cells from individual mice treated with VEH (n = 4), RPM (n = 6), and TAC (n = 6) in cohorts 3 and 4, 30 days post-drug cessation. (J and K) Cumulative persistence of peripheral syngeneic 4CAR-T cells and allogeneic HLA$^+$ 4CAR-T cells during the drug treatment interval (1–13 days post-infusion) (J) and post-drug cessation (22–42 days post-infusion) (K). For all data, symbols and sample sizes indicate biologically independent animals. Bars and lines represent mean and error bars show ±SEM. Statistical significance was calculated by Kruskall-Wallace test with Dunn's test for multiple comparisons (C and D), Spearman correlation (E and F), Wilcoxon matched pairs signed rank test (G and I), and Wilcoxon rank-sum test (J and K). AUC, area under the curve; r, coefficient of correlation.

degree as syngeneic 4CAR-T cells within individual mice until 1 week post-T cell infusion, while allogeneic HLA$^+$ 4CAR-T cells from TAC-treated mice persisted similarly to their syngeneic counterparts for the entire drug treatment interval (Figures 3D and S8). Moreover, the extent of circulating allogeneic HLA$^+$ 4CAR-T cell preservation positively correlated with the contemporaneous trough plasma

concentration of RPM and TAC (Figures 3E and 3F). Mice from cohort 5 were then euthanized at 1 day post-drug withdrawal to determine if TAC treatment inhibited allorejection in tissue. We detected equivalent levels of allogeneic HLA$^+$ and HLA-deficient 4CAR-T cells from spleens of TAC-treated mice, whereas HLA$^+$ 4CAR-T cells from VEH-treated mice were depleted (Figure 3G). Notably, following drug treatment cessation in mice from cohorts 3 and 4, allogeneic HLA$^+$ 4CAR-T cells were swiftly eliminated from circulation (Figure S9), and when mice were euthanized 30 days after drug withdrawal these cells were nearly undetectable in tissue, indicating recovery of host immunologic rejection (Figures 3H and 3I). At the given dosages, TAC more than RPM improved cumulative allogeneic HLA$^+$ 4CAR-T cell persistence during the drug treatment interval (Figure 3J) and post-drug withdrawal (Figure 3K). These data demonstrated that RPM and TAC treatment extended the *in vivo* lifespan of allogeneic HLA$^+$ 4CAR-T cells upon transfer into HLA-mismatched HIS mice.

Genetic disruption of *FKBP1A* renders CAR-T cells resistant to RPM and TAC

To overcome RPM- and TAC-mediated impairment of CAR-T cell function, we engineered immunosuppressant-resistant CAR-T cells by disrupting the gene encoding FKBP prolyl isomerase 1A (*FKBP1A*), which is an intracellular binding partner of RPM and TAC.[15] *FKBP1A*-specific single-guide RNAs (sgRNAs) (Table S1) were paired with mRNA encoding either an adenosine (ABE8.20m) or cytosine (BE4) base editor and electroporated into activated primary human T cells (Figure 4A). This screen identified an ABE8.20m-sgRNA (TSBTx1538) pair targeting an intron-exon splice junction that achieved a mean on-target genomic editing efficiency of 93.7% (Figure 4B) and reduced FKBP1A protein expression (Figure S10). Following activation, *FKBPIA*^{KO} T cells treated with RPM retained phosphorylation of the S6 ribosomal protein, a downstream substrate of the PI3K/Akt/mTOR pathway (Figures 4C and 4D), and maintained calcineurin-induced NFAT-driven GFP expression after TAC treatment (Figures 4E and 4F) indicating that *FKBP1A*^{KO} restores proximal signaling events inhibited by these immunosuppressants.

To evaluate whether *FKBP1A*^{KO} confers T cells with functional resistance to immunosuppression, we stimulated CD19-specific CAR-T cells (19CAR) with JeKo-1 mantle cell tumors in the presence of RPM, TAC, or VEH. Under immunosuppression, both *FKBP1A*^{KO} CD4$^+$ and CD8$^+$ 19CAR-T cells proliferated greater than unmodified 19CAR-T cells and, notably, expanded to a similar extent as their VEH-treated counterparts (Figure 4G). Furthermore, immunosuppressant treatment also drastically reduced the frequency of unmodified 19CAR-T cells producing GM-CSF, IL-2, IFN-γ, and TNF-α, while the magnitude of cytokine-positive *FKBP1A*^{KO} 19CAR-T cells remained unchanged from VEH treatment (Figures 4H and 4I). *FKBP1A*^{KO} 19CAR-T cells also overcame RPM and TAC inhibition to eradicate GFP$^+$ JeKo-1 tumor cells *in vitro* with nearly the same kinetics as treatment with VEH. In contrast, immunosuppressants diminished the ability of unmodified 19CAR-T cells to control tumor growth (Figures 4J, S11, and S12).

In addition, we evaluated whether *FKBP1A*^{KO} rendered 19CAR-T cells resistant to corticosteroids, a treatment option for patients experiencing adverse events following CAR-T cell therapy.[37–39] Both dexamethasone and prednisone suppressed pro-inflammatory cytokine secretion and antigen-driven proliferation of *FKBP1A*^{KO} 19CAR-T cells (Figure S13), indicating that *FKBP1A*^{KO} does not interfere with steroid-mediated suppression. Collectively, these findings support that genetic ablation of *FKBP1A* renders CAR-T cells resistant to RPM- and TAC-induced inhibition.

FKBP1A^{KO} 19CAR-T cells resist immunosuppression to control *in vivo* tumor progression

To evaluate whether *FKBP1A*^{KO} 19CAR-T cells resisted immunosuppression *in vivo*, we transplanted luciferase-expressing JeKo-1 tumors into NSG mice and 1 week later initiated RPM, TAC, or VEH treatment daily for 2 weeks. One day post-treatment initiation, mice were infused with either *FKBP1A*^{KO} or unmodified 19CAR-T cells, or untransduced (UTD) control T cells (Figure 5A). Both 19CAR-T cell populations eradicated tumors in VEH-treated mice relative to mice that received UTD T cells. TAC treatment attenuated the ability of unmodified 19CAR-T cells to control tumor outgrowth, whereas *FKBP1A*^{KO} CAR-T cells potently suppressed tumor progression under TAC (Figures 5B and 5C). Moreover, during the TAC treatment interval *FKBP1A*^{KO} 19CAR-T cells drastically reduced cumulative tumor burden equivalent to unmodified 19CAR-T cells in VEH-treated mice (Figure 5D), indicating that *FKBP1A*^{KO} confers 19CAR-T cell resistance to TAC inhibition *in vivo*.

Unlike TAC treatment, RPM administration mitigated JeKo-1 growth in control mice, which obscured our ability to detect additive anti-tumor benefit in mice receiving *FKBP1A*^{KO} over unmodified 19CAR-T cells (Figure 5E). This observation is consistent with B cell malignancies exhibiting constitutive PI3K/Akt/mTOR pathway activation[40,41] and sensitivity to mTOR inhibitors.[42,43] Indeed, RPM treatment attenuated protein phosphorylation of mTOR and downstream substrates S6 and 4EBP1, as well as inhibited *in vitro* proliferation of JeKo-1, Raji, and Nalm6 cancer cell lines (Figure S14). To overcome this obstacle, we generated *FKBP1A*^{KO} JeKo-1 tumors that, when in the presence of RPM, exhibited comparable *in vivo* expansion kinetics to when they are treated with VEH (Figure 5F). Using *FKBP1A*^{KO} JeKo-1 tumors, we now demonstrated that *FKBP1A*^{KO} 19CAR-T cells, not unmodified 19CAR-T cells, decreased cumulative tumor burden within the RPM treatment interval to the same extent as in VEH-treated mice (Figure 5G). These data demonstrated that *FKBP1A*^{KO} 19CAR-T cells effectively resist immunosuppression and exhibit robust *in vivo* anti-tumor activity.

HLA-mismatched *FKBP1A*^{KO} 19CAR-T cells and TAC treatment overcome rejection to induce B cell aplasia *in vivo*

Finally, we assessed whether immunosuppressant treatment mitigates *in vivo* rejection of allogeneic HLA$^+$ *FKBP1A*^{KO} 19CAR-T cells to an extent that permits functional immune responses. Here, we leveraged the endogenous B cell compartment of HIS mice as an on-target population for 19CAR-T cells, where both the depth of

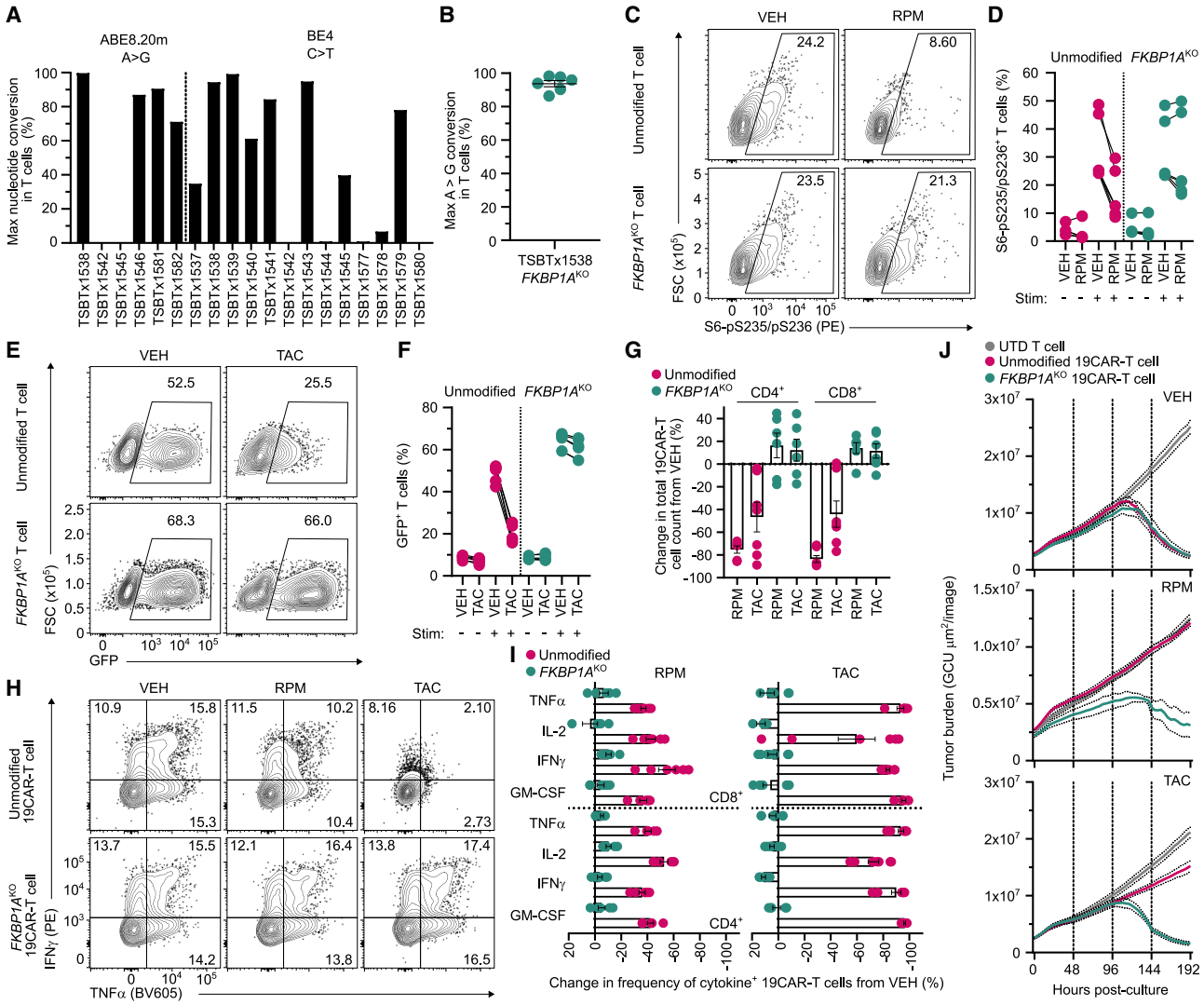

Figure 4. *FKBP1A*-disrupted CAR-T cells resist rapamycin and tacrolimus immunosuppression *in vitro*

(A) Frequency of maximum on-target nucleotide conversion by next-generation sequencing (NGS) in T cells base edited with individual *FKBP1A*-specific sgRNAs complexed with mRNA encoding an adenosine (ABE8.20m) or cytosine (BE4) base editor. (B) Frequency of maximum on-target A>G nucleotide conversion by NGS in T cells base edited with TSBTx1538 sgRNA and ABE8.20m mRNA (*FKBP1A*^{KO}). Symbols indicate independent donors. (C and D) FACS plots (C) and summarized data (D) indicate frequency of phosphorylated S6 protein in unmodified and *FKBP1A*^{KO} T cells that were activated and treated with rapamycin (RPM) or DMSO vehicle (VEH) control. (E and F) FACS plots (E) and summarized data (F) indicate frequency of NFAT-driven GFP expression in reporter T cells that were unmodified or *FKBP1A*^{KO} after treatment with tacrolimus (TAC) or VEH. (G) Percentage change in total CD19-specific CAR-T cells (19CAR) counts 1 week post-treatment with RPM or TAC relative to VEH. Symbols represent three independent donors in duplicate. (H and I) Intracellular cytokine expression was measured in unmodified and *FKBP1A*^{KO} 19CAR-T cells after stimulation with JeKo-1 tumor cells in the presence of RPM, TAC, or VEH. FACS plots indicate frequency of IFN-γ$^+$ and TNF-α$^+$ 19CAR-T cells (H) and summarized data show percentage change in cytokine expression in RPM- and TAC-treated conditions relative to VEH (I). (J) Incucyte cytotoxicity assay as described in materials and methods. Tumor burden quantified as green calibrated units (GCUs) derived from the fluorescence intensity of GFP$^+$ JeKo-1 tumors that were cultured in triplicate with either untransduced (UTD) T cells, unmodified 19CAR-T cells, or *FKBP1A*^{KO} 19CAR-T cells at a 0.25:1 ratio. Solid lines represent mean GCU from images taken every 4 h, dotted lines show ±SEM, and vertical lines indicate redosing with VEH, RPM, or TAC. (D, F, and I) Symbols represent three independent donors in duplicate. For all data, lines and bars represent mean and error bars show ±SEM.

B cell aplasia and the persistence of allogeneic cells could assess treatment efficacy. HIS mice from four HLA-mismatched cohorts (6–9) were allocated into groups that received UTD T cells and VEH treatment (group 1), HLA$^+$ *FKBP1A*^{KO} 19CAR-T cells and VEH treatment (group 2), HLA$^+$ *FKBP1A*^{KO} 19CAR-T cells and TAC treatment (group 3), and HLA-deficient 19CAR-T cells and VEH treatment (group 4) (Figure 6A). Given that allogeneic HLA-deficient T cells evade rejection in HIS mice (Figures 1G

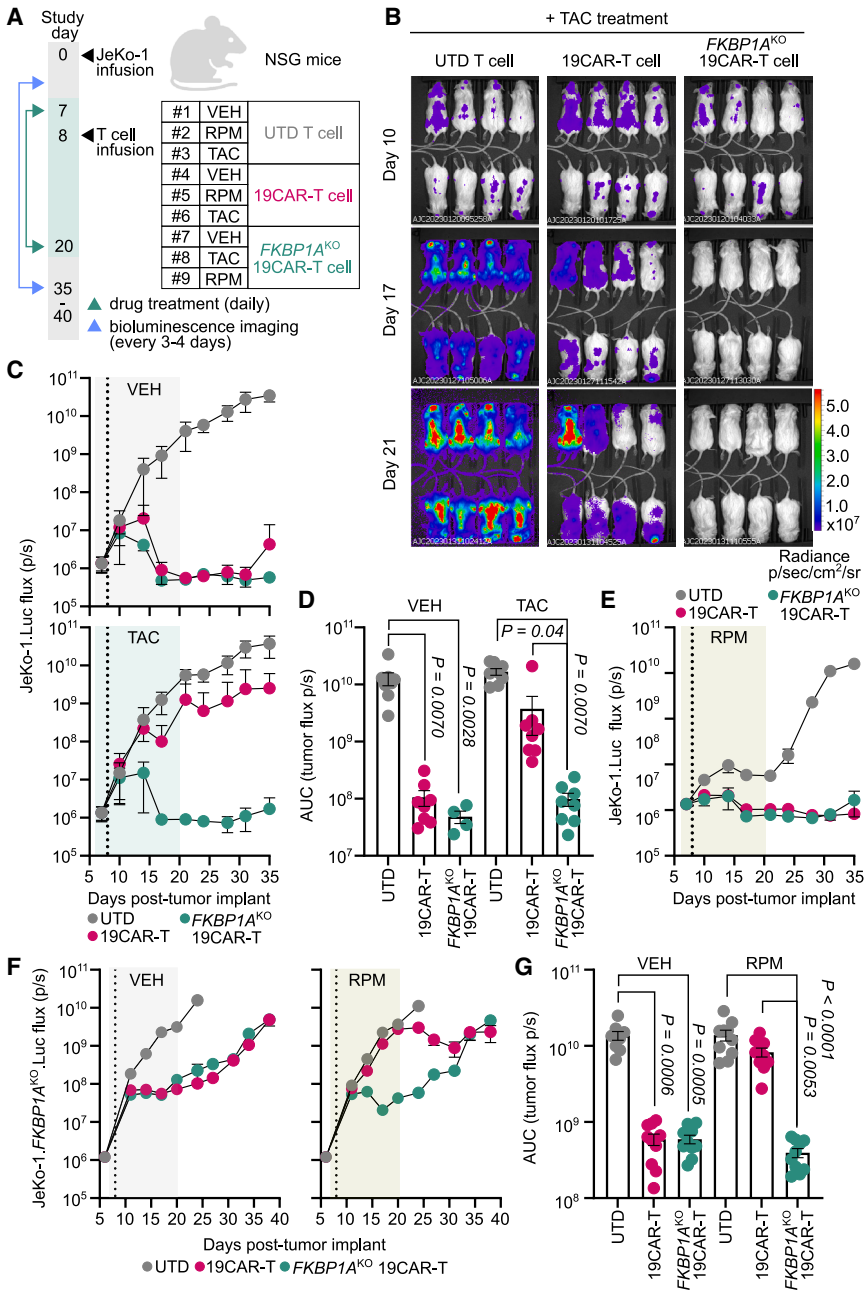

Figure 5. *FKBP1A*^{KO} 19CAR-T cells retain *in vivo* anti-tumor function in the presence of tacrolimus and rapamycin

(A) Schematic of drug treatment in xenograft tumor-bearing mouse model for (B)–(E). JeKo-1.Luc cells (5×10^5) were transplanted into recipient NSG mice (n = 72), then 7 days later mice initiated vehicle (VEH) (n = 24), rapamycin (RPM) (n = 24), or tacrolimus (TAC) (n = 24) treatment daily for 2 weeks. One day later, mice from each treatment group were infused with 1×10^6 untransduced (UTD) T cells (n = 8 per group), unmodified CD19-specific CAR-T cells (19CAR) (n = 8 per group), or *FKBP1A*^{KO} 19CAR-T cells (n = 8 per group). (B) Representative longitudinal bioluminescent flux imaging of JeKo-1.Luc-bearing NSG mice treated with TAC and UTD, 19CAR, or *FKBP1A*^{KO} 19CAR-T cells. (C) Longitudinal tumor burden (flux p/s) of T cell-treated mice that received VEH or TAC treatment. (D) Cumulative tumor burden of T cell-infused mice during the VEH or TAC treatment interval. (E) Longitudinal tumor burden of T cell-infused mice that received VEH or RPM treatment. (F and G) NSG mice were implanted with 5×10^5 JeKo-1.*FKBP1A*^{KO}.Luc cells and 6 days later initiated VEH (n = 30) or RPM (n = 30) treatment daily for 2 weeks. One day after, mice from each treatment group were infused with either 1×10^6 UTD T cells (n = 10 per group), unmodified 19CAR-T cells (n = 10 per group), or *FKBP1A*^{KO} 19CAR-T cells (n = 10 per group). (F) Longitudinal tumor burden of T cell-infused mice that received VEH or RPM treatment. (G) Cumulative tumor burden of T cell-infused mice during the VEH or RPM treatment interval. (C, E, and F) Vertical dotted line indicates T cell infusion. For all data, symbols and bars reflect means and error bars show ±SEM, except (D) and (G), where symbols represent individual mice. Sample sizes represent biologically independent animals. Statistical significance was calculated by Kruskall-Wallace test with Dunn's test for multiple comparisons (D and G). AUC, area under the curve.

and 1H), these cells served as a benchmark to measure the effectiveness of TAC and allogeneic HLA$^+$ 19CAR-T cell therapy (group 3). Upon infusion, we observed that TAC and *FKBP1A*^{KO} 19CAR-T cell-treated mice (group 3) exhibited lower CD19$^+$ B cell counts in peripheral blood (Figures 6B and 6C), spleen (Figure 6D), and bone marrow (Figure 6E) compared with VEH-treated mice (group 2), and to a near-equivalent level in mice treated with HLA-deficient 19CAR-T cells (group 4). We also measured a significant reduction in CD19 surface density on residual B cells (Figure 6F) and emergence of CD19^{dim}CD22$^+$ B cells (Figure 6G) from mice in group 3 compared with the group 2 control, indicating effective selection pressure by HLA$^+$ *FKBP1A*^{KO} 19CAR-T cells in the presence of TAC. Furthermore, allogeneic HLA$^+$ *FKBP1A*^{KO} 19CAR-T cells from TAC-treated mice (group 3) persisted in peripheral blood (Figures 6H and 6I) and spleen (Figure 6J) to a similar magnitude as HLA-deficient 19CAR-T cells (group 4). Together, these data demonstrate that TAC treatment confers allogeneic HLA$^+$ *FKBP1A*^{KO} CAR-T cells sufficient protection from immunologic rejection to deplete endogenous B cells.

DISCUSSION

Here, we describe a strategy where allogeneic, universal donor-derived CAR-T cells in the presence of immunosuppressant treatment persist and retain effector function in humanized mice.

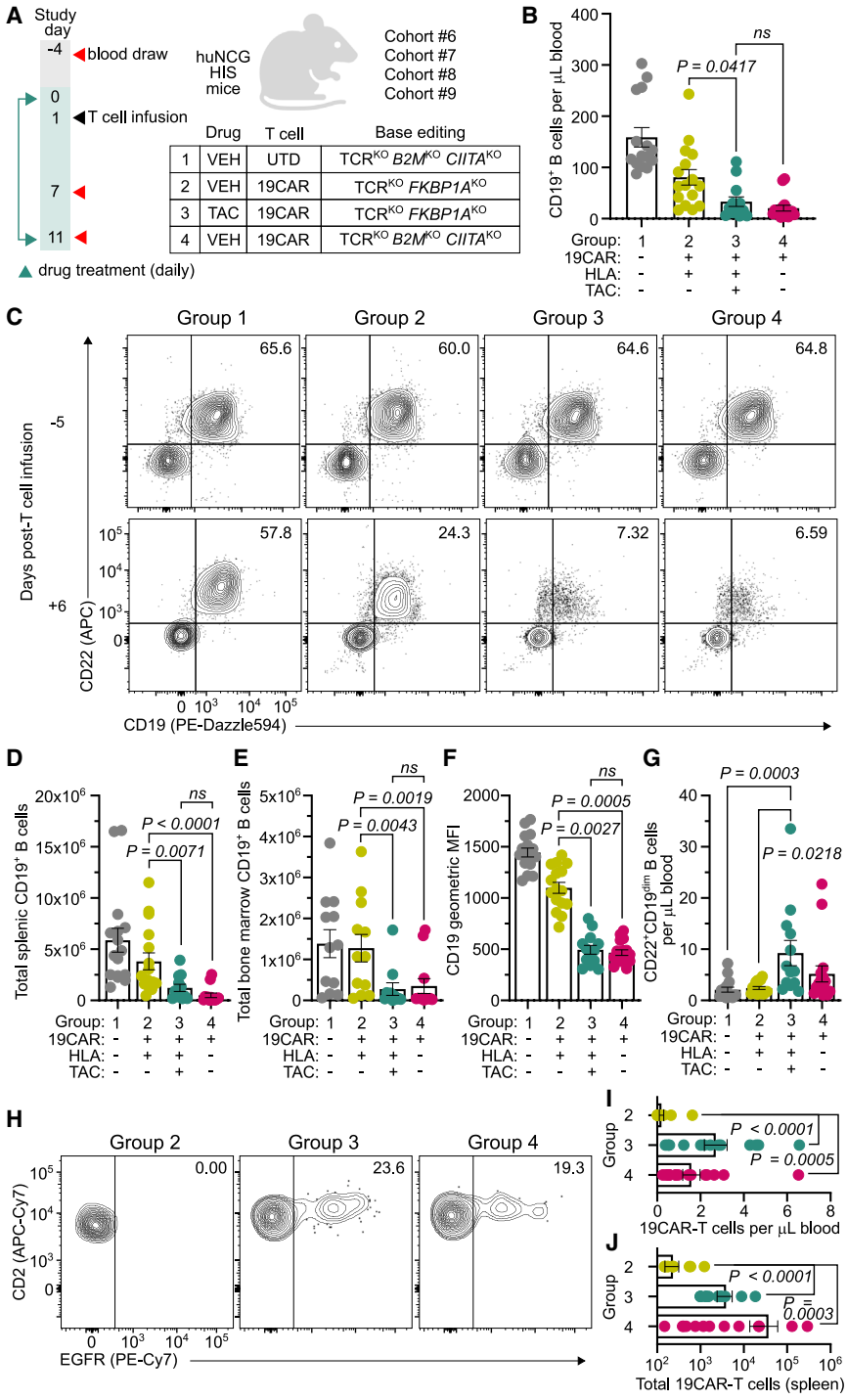

Figure 6. Allogeneic *FKBP1A*^{KO} 19CAR-T cells induce B cell aplasia in tacrolimus-treated HIS mice

(A) Four independent cohorts (6–9) of huNCG HIS mice were evenly distributed into groups: group 1 (n = 16) received allogeneic HLA-deficient (*B2M*^{KO}*CIITA*^{KO}) UTD T cells and VEH treatment, group 2 (n = 16) received allogeneic HLA$^+$ CD19-specific CAR-T cells (19CAR) and VEH treatment, group 3 (n = 15) received allogeneic HLA$^+$ *FKBP1A*^{KO} 19CAR-T cells and TAC treatment, and group 4 (n = 16) received allogeneic HLA-deficient 19CAR-T cells and VEH treatment. All T cells were base edited to disrupt TCR expression. (B and C) Concentration (B) and FACS plots indicate frequency (C) of peripheral CD19$^+$ B cells 6 days post-T cell infusion from mice in groups 1–4. (D and E) Total CD19$^+$ B cells from individual mouse splenic (D) and bone marrow (E) tissue 10 days post-T cell infusion in groups 1–4. (F) Geometric median fluorescent intensity (MFI) of CD19 expression on peripheral CD22$^+$ B cells 6 days post-T cell infusion from mice in groups 1–4. (G) Concentration of peripheral CD22$^+$CD19^{dim} B cells 6 days post-T cell infusion from mice in groups 1–4. (H) FACS plots indicate frequency of EGFR$^+$ 19CAR-T cells from mice in groups 2–4, 10 days post-T cell infusion. (I and J) Peripheral concentration of 19CAR-T cells (I) and total splenic 19CAR-T cells (J) from mice in groups 2–4, 10 days post-T cell infusion. For all data, bars reflect mean, error bars show ±SEM, and symbols indicate biologically independent animals. Statistical significance was calculated by Wilcoxon rank-sum test (B, D, and E) and Kruskall-Wallace test with Dunn's test for multiple comparisons (F, G, I, and J).

Allogeneic CAR-T cells were base edited to inactivate the T cell receptor complex preventing GVHD, and critically, *FKBP1A*, which conferred robust resistance to RPM and TAC suppression. Simultaneous immunosuppressant therapy was necessary to mitigate recipient immune-driven rejection of HLA-mismatched CAR-T cells, whereafter drug withdrawal allogeneic CAR-T cells were eliminated. This strategy demonstrates that genome engineering enables immunosuppressants to increase the therapeutic potential of allogeneic CAR-T cells by overcoming allorejection.

Reconstitution of the patient immune system following lymphodepleting chemotherapy accelerates rejection of allogeneic CAR-T cells, which may limit durable responses and overall treatment efficacy. Previous reports describe complex genome engineering strategies to limit alloreactivity. For example, simultaneous disruption of *B2M* and *CIITA* abrogate recognition by recipient CD8$^+$ and CD4$^+$ T cells, respectively.[8,9] However, HLA deficiency necessitates additional intervention to evade or inhibit NK cell killing, including deletion of adhesion molecules (e.g., CD54 and CD58)[44] and activating ligands (e.g., CD155),[45] or overexpression of inhibitory ligands (e.g., HLA-E,[30–32,45] HLA-G,[30,46] CD47,[46,47] PD-L1[46]). Indeed, enhanced resistance to allorejection has been observed, but only after combining multiplex gene editing with forced expression of protective

transgenes.[30–32,45–47] Instead, single genetic disruption of *FKBP1A* with an adenosine base editor simplifies the genome engineering strategy, which may ultimately mitigate the extent of genomic abnormalities associated with CRISPR-Cas9-induced double-strand DNA breaks[48–50] and alleviate lentiviral[51] or AAV[52] vector packaging constraints resulting from the delivery of multiple transgenes.

We first demonstrated that genetic disruption of HLA surface expression on allogeneic CAR-T cells effectively prevented recognition by recipient T cells but sensitized them to NK cell-driven attack due to missing self-recognition. We observed that reconstitution of HLA-I single-chain molecules into *B2M*^{KO} T cells conferred marginal protection against NK cell lysis. This effect was likely due to the insufficient frequency of NK cell subsets expressing the corresponding inhibitory KIR or NKG2A. Instead, allogeneic T cells that fully maintained HLA-I surface expression resisted rejection by NK cells, which we also observed *in vivo* using huNK mice. Given the extensive diversity of HLA and KIR alleles between unrelated donor-recipient pairs,[36] this finding suggests that allogeneic HLA-I^{+} CAR-T cells are best capable to broadly inhibit recipient NK cells by reducing the probability of KIR/KIR-ligand mismatch. Moreover, it may be highly advantageous to pre-select allogeneic donors based on HLA genotype. In this way, donors that express KIR-ligands, HLA-Bw4, HLA-C1, and HLA-C2 alleles, are poised to inhibit diverse populations of KIR^{+} NK cells.

To protect HLA^{+} CAR-T cells after infusion into HLA-mismatched HIS mice, we co-administered immunosuppressants to mitigate allorejection. RPM and TAC interact with FKBP1A to inhibit mTOR[16–18] or calcineurin activation,[19] respectively, and are routinely used to prevent GVHD in the allogeneic hematopoietic stem cell transplant (HSCT) setting.[13,14] During the treatment interval, TAC over RPM improved the persistence of allogeneic HLA^{+} CAR-T cells to a level equivalent to syngeneic HIS mouse-derived CAR-T cells. Their degree of persistence correlated with the contemporaneous trough plasma concentration of TAC (1–3 ng mL^{-1}), which was lower than the drug target exposure in humans post-HSCT (5–20 ng mL^{-1}).[13] Unlike TAC, RPM treatment significantly inhibited B cell tumor progression, which is consistent with RPM analogs exhibiting single-agent activity in patients with aggressive lymphomas.[53,54] Together, this suggests an opportunity to augment therapeutic efficacy by leveraging anti-rejection and anti-tumor benefits of these immunosuppressants with allogeneic *FKBP1A*^{KO} 19CAR-T cells.

The optimal duration of allogeneic CAR-T cell persistence will likely depend on the disease indication. However, transient treatment with RPM or TAC, not long-term exposure, may be sufficient to facilitate meaningful CAR-T cell-driven responses while minimizing side effects associated with immunosuppression. In the autologous CAR-T cell setting, deeper initial remissions and higher peak CAR-T cell expansion are associated with improved patient outcomes.[55] These clinical observations combined with the kinetics of both cellular immune reconstitution and CAR-T cell expansion could inform the duration of immunosuppressant treatment. For example, patient CD8^{+} T cells recover at a median time of 21 days post-lymphodepletion,[56] meanwhile peak CAR-T cell expansion generally occurs by 3 weeks post-infusion.[37,57,58] These findings imply that transient immunosuppressant treatment, possibly 3–4 weeks, around the time of immune reconstitution would be critical to inhibit allorejection, thereby permitting unhindered expansion of allogeneic CAR-T cells to drive deep initial responses. Utilizing short-term immunosuppressant treatment to maximize the initial response may also be advantageous against autoimmune diseases, where transient peripheral engraftment of 19CAR-T cells can induce remission of systemic lupus erythematosus.[59] During this treatment interval, patients would likely be monitored for trough drug concentrations to avoid increased risk of allograft rejection or toxicity if drug levels were too low or high, respectively. Furthermore, CAR-T cell patients are infection prone[60] and immunosuppressant therapy may exasperate this risk, which could necessitate enhanced monitoring or even prophylaxis to manage these complications.

In these studies, we used a 2-week drug treatment interval as proof-of-principle, although allogeneic CAR-T cells were infused into lymphoreplete mice without prior conditioning that would otherwise be performed in humans. Despite pre-existing endogenous T cells, HLA-mismatched *FKBP1A*^{KO} 19CAR-T cells coupled with TAC induced B cell aplasia to the same extent as their HLA-deficient counterparts. Although not directly evaluated in our study, immunosuppressant-mediated suppression of host anti-tumor immune responses could be an undesired consequence given that endogenous immunity can contribute to favorable outcomes in the post-CAR-T cell therapy setting.[61,62] However, immunosuppressants may compensate for the loss of endogenous T cell and NK cell responses by exerting anti-tumor activity through indirect and direct pathways. For example, TAC may remodel the tumor microenvironment and remove tumor-support mechanisms by preventing formation of neutrophil extracellular traps,[63] mitigating M2 polarization of pro-fibrotic macrophages,[64,65] and destabilizing regulatory T cell identity.[66–68] Meanwhile, single-agent use of the rapalog temsirolimus in patients with renal cell carcinoma improved survival outcomes compared with treatment with IFN-α,[69,70] which exhibits potent immune-stimulatory activity. Furthermore, steroid-resistant CAR-T cells with concurrent dexamethasone treatment induced localized tumor regression and necrosis in glioblastoma patients.[71] Together, these findings provide examples where treatment with immunosuppressants alone or in combination with CAR-T cells exhibit meaningful clinical responses in the absence of endogenous immunity. Careful consideration should be given to utilizing these drugs in combination with *FKBP1A*^{KO} CAR-T cells for a given disease, where their combined contribution may outweigh the anti-tumor benefit of endogenous immune responses.

Immunosuppressant treatments and cellular immunotherapies have coincided at an increasing rate, highlighting the practical utility of their interaction for diverse applications.[71–74] We demonstrated that *FKBP1A*^{KO} CAR-T cells are resistant to RPM and TAC, and both drugs mitigate allorejection in a stringent humanized

small-animal model. Importantly, this demonstration may afford healthcare providers flexibility to develop patient-specific treatment plans or adjust drug selection and treatment duration in response to the patient's condition. In particular, drug cessation potentially could be leveraged to manage treatment-related adverse events, prevent long-term B cell aplasia, or reduce the risk of aberrant clonal outgrowth that may arise from genome engineering.[75,76] Collectively, these findings indicate that immunosuppressant treatment extends the *in vivo* lifespan of HLA-mismatched CAR-T cells offering promise that allogeneic cell therapies can achieve autologous cell-like persistence and associated clinical responses.

MATERIALS AND METHODS

Ethics

BLT (bone marrow, liver, thymus) humanized mice were produced using anonymous human fetal tissue (gestational age of 17–19 weeks) acquired from healthy donors with informed consent by Advanced Bioscience Resources and used under approved protocols from Partners Healthcare Institutional Review Board. BLT mouse experiments were conducted at the Ragon Institute of Mass General, MIT and Harvard, and were approved by the Massachusetts General Hospital Institutional Animal Care and Use Committee (IACUC) under the protocol 2021N000279. NSG, NSG-IL-15tg, and humanized $CD34^+$ NCG mouse studies were performed at the Charles River Accelerator and Development Lab (CRADL) and were approved by the CRADL IACUC under protocol 2021-1298. Animal studies were performed following the instructions in the NIH Guide for the Care and Use of Laboratory Animals.

Humanized immune system mice

BLT humanized mice were generated from female (aged 6–8 weeks) NOD.Cg-*Prkdc*^{scid}*IL2rg*^{tm1Wjl}/*SzJ* (NSG) mice (Jackson Laboratory) as described previously.[77] In brief, NSG mice were anesthetized and whole-body irradiated (2 Gy), and then implanted with 1 mm^3 fragments of human fetal liver and thymus tissue beneath the murine kidney capsule. Subsequently, 1×10^5 autologous fetal liver-derived $CD34^+$ stem cells were intravenously injected within 6 h of transplantation. Beam Therapeutics obtained female NOD-*Prkdc*^{em26Cd52}*IL2rg*^{em26CD22}/*NjuCrl* (NCG) $CD34^+$ humanized (huNCG) mice from Charles River and female (aged 6–8 weeks) NSG-Tg(IL15)1Sz/SzJ (NSG-IL15tg) mice from Jackson Laboratory. huNCG mice were generated from female (aged 4–6 weeks) NCG mice that were myeloablated and then intravenously infused with human umbilical cord blood-derived $CD34^+$ stem cells from a qualified source. huNK mice were generated by supplementing the water of NSG-IL-15tg with Baytril (Bayer) for 1 week followed by whole-body irradiation (2 Gy). Primary human $CD56^+$ NK cells (5×10^6) were then intravenously injected 24 h later. At the Ragon Institute and CRADL, mice were housed in microisolator cages and fed autoclaved food and water. Animal rooms were maintained at 72°F ± 2°F, 30%–70% relative humidity, and were on a 12:12 h light/dark cycle. Human reconstitution was assessed from 12 to 17 weeks post-transplant in BLT and huNCG mice, and 2–3 weeks post-transplant in huNK mice. Mice were included in studies when ≥25% of blood cells in the lymphocyte gate were human $CD45^+$ in BLT and huNCG mice, and when human $CD56^+$ cells achieved 10 cells μL^{-1} blood in huNK mice.

In vivo drug formulation

RPM (Thermo Fisher Scientific) and TAC (Cayman Chemical) were reconstituted in DMSO (Sigma-Aldrich) at 10 and 25 mg mL^{-1}, respectively, and 0.22 μm sterile filtered. RPM was diluted to 0.15 mg mL^{-1} and TAC was diluted to 1.5 mg mL^{-1} using sterile-filtered VEH solution comprising a 1:1 ratio of 5% (v/v) polyethylene glycol (Sigma-Aldrich) and 5% (v/v) Tween 80 (Sigma-Aldrich). PEG-Tween solution served as VEH control and percent volume DMSO was normalized across all treatments.

HIS mouse-driven allorejection model

For the study described in Figure S1, BLT mice ($n = 3$) were intravenously injected with 5×10^6 syngeneic BLT mouse-derived CD4-based CAR-T cells (4CAR) and 5×10^6 allogeneic human donor-derived 4CAR-T cells. For Figures 1F–1I, BLT mice ($n = 6$) were infused with an allogeneic human donor-derived T cell product comprising 5×10^6 TCR^{KO} 4CAR-T cells and 5×10^6 $TCR^{KO}B2M^{KO}CIITA^{KO}$ 4CAR-T cells. All mice were bled through puncture of the retro-orbital sinus 1 day post-infusion and weekly thereafter until necropsy at day 21 (Figure S1) or day 60 (Figures 1F–1I) when various tissues were collected to analyze 4CAR-T cells.

For Figure 3, BLT mice were used in cohort 2 ($n = 12$) and cohort 5 ($n = 13$), and huNCG mice were used in cohort 1 ($n = 10$), cohort 3 ($n = 12$), and cohort 4 ($n = 10$). HIS mice from each cohort were allocated into groups via matched distribution based on human T cell reconstitution (cells μL^{-1} blood) using StudyLog software (Studylog Systems) and received daily intraperitoneal injections of RPM (1 mg kg^{-1}), TAC (10 mg kg^{-1}), or VEH control for 14 days. Each mouse cohort represented an independent study where mice in cohort 1 received VEH ($n = 5$) or RPM ($n = 5$); cohort 2 received VEH ($n = 5$) or RPM ($n = 7$); cohort 3 received VEH ($n = 4$), RPM ($n = 4$), or TAC ($n = 4$); cohort 4 received VEH ($n = 4$), RPM ($n = 3$), or TAC ($n = 3$); and cohort 5 received VEH ($n = 7$) or TAC ($n = 6$). One day post-drug treatment initiation, HIS mice were intravenously infused with a unique allogeneic human donor-derived T cell product comprising 5×10^6 TCR^{KO} 4CAR-T cells and 5×10^6 $TCR^{KO}B2M^{KO}CIITA^{KO}$ 4CAR-T cells. Mice in cohorts 3 and 4 were also infused with 5×10^6 syngeneic HIS mouse-derived 4CAR-T cells. Persistence of 4CAR-T cells was monitored at 1 day post-T cell infusion and approximately weekly thereafter via blood draws from the retro-orbital sinus or submandibular vein. HIS mice in cohort 5 were necropsied 24 h after final drug treatment and tissues were collected to analyze 4CAR-T cells.

For Figure 6, huNCG mice were used in cohort 6 ($n = 16$), cohort 7 ($n = 12$), cohort 8 ($n = 24$), and cohort 9 ($n = 12$) and were evenly distributed into four groups via matched distribution based on human T cell reconstitution. HIS mice in group 1 received VEH and

5×10^6 TCR^{KO}*B2M*^{KO}*CIITA*^{KO} UTD T cells, group 2 received VEH and 5×10^6 TCR^{KO}*FKBP1A*^{KO} CD19-specific CAR-T cells (19CAR), group 3 received TAC and 5×10^6 TCR^{KO}*FKBP1A*^{KO} 19CAR-T cells, and group 4 received VEH and 5×10^6 TCR^{KO}*B2M*^{KO}*CIITA*^{KO} 19CAR-T cells. HIS mice were treated daily with TAC (10 mg kg^{-1}) or VEH for 11 days via intraperitoneal injections and at 1 day post-drug treatment initiation mice were intravenously infused with T cells derived from an allogeneic human donor. Endogenous B cell aplasia and persistence of 19CAR-T cells was monitored at 7 and 11 days post-drug treatment via blood draw from the submandibular vein and tissue collection at necropsy.

When available, HLA typing was performed on genomic DNA isolated from whole blood of HIS mice and from purified allogeneic donor T cells (Table S2). Genomic DNA was isolated with QIAamp DNA Blood Mini Kit (QIAGEN) using the manufacturer's instructions and submitted to Scisco Genetics for HLA class I typing using ScisGo-HLA-v6 next-generation sequencing technology.

NK cell rejection models

For the study described in Figure S4, BLT mice (n = 13) received intraperitoneal injections every 2–3 days of 2.5 μg recombinant human IL-15 (BioLegend) or sterile PBS (n = 6) for 6 total injections. Subsequently, IL-15-treated (n = 6) and PBS-treated (n = 4) mice were intravenously infused with an allogeneic human donor-derived T cell product comprising 5×10^6 TCR^{KO} 4CAR-T cells and 5×10^6 TCR^{KO}*B2M*^{KO}*CIITA*^{KO} 4CAR-T cells. Persistence of 4CAR-T cells was monitored at 1, 4, and 7 days post-T cell infusion via blood draw from the retro-orbital sinus. For the study described in Figures 1L–1N, huNK cell mice (n = 5) and unreconstituted NSG-IL-15tg control mice (n = 5) were intravenously infused with an allogeneic human donor-derived T cell product comprising 5×10^6 TCR^{KO} 4CAR-T cells and 5×10^6 TCR^{KO}*B2M*^{KO}*CIITA*^{KO} 4CAR-T cells. Persistence of 4CAR-T cells was monitored at 1, 4, and 7 days post-T cell infusion via blood draw from submandibular vein.

Anti-tumor efficacy model

For the study described in Figures 5A–5E, NSG mice were intravenously injected with 5×10^5 JeKo-1.Luc cells at day 0. On day 7, mice initiated daily intraperitoneal injections of VEH, RPM (1 mg kg^{-1}), or TAC (10 mg kg^{-1}) for 2 weeks. Mice from each treatment cohort were injected on day 8 with 1×10^6 UTD T cells, unmodified 19CAR-T cells, or *FKBP1A*^{KO} 19CAR-T cells (n = 8 per group). For the study described in Figures 5F and 5G, NSG mice were intravenously injected with 5×10^5 JeKo-1.*FKBP1A*^{KO}.Luc cells at day 0. On day 7, mice initiated daily intraperitoneal injections of VEH or RPM (1 mg kg^{-1}) for 2 weeks. Mice from each treatment cohort were injected on day 8 with 1×10^6 UTD T cells, unmodified 19CAR-T cells, or *FKBP1A*^{KO} 19CAR-T cells (n = 10 per group). For all studies, tumor burden was measured every 3–4 days post-tumor implant by bioluminescence imaging (IVIS Spectrum, Spectral Instruments Imaging) 30 min after intraperitoneally injecting mice with 150 mg kg^{-1} XenoLight D-Luciferin (PerkinElmer). The acquisition time was automatically determined by the instrument for each exposure, and quantification of flux from imaging datasets was performed with the Living Image Studio software (PerkinElmer). In brief, a constant region of interest was drawn over the mouse and flux was reported as total photon per second.

Mass spectrometry

For the study described in Figures 3E and 3F, plasma concentrations of RPM and TAC were determined using liquid chromatography-mass spectrometry (LC-MS). Mouse plasma from whole blood 1 week post-T cell infusion was isolated by centrifugation (2,200 × *g*, 5 min, 4°C) and then cryopreserved. Thawed samples were injected into an Agilent Infinity 1290 II liquid chromatography coupled with a ScieX 6500+ triple quad mass spectrometer. In brief, the sample plasma, calibration curve (CC), and quality control (QC) samples were prepared by aliquoting 5 μL per sample into a 96-well plate. CC standards (0.5, 1, 5, 25, 100, 500, 900, and 1,000 ng mL^{-1}) and QC samples (1.5, 75, and 750 ng mL^{-1}) were prepared in mouse plasma (BioIVT). Tolbutamide (10 ng mL^{-1}) in acetonitrile was the internal standard and 100 μL was added per well except the wells containing 5 μL blank mouse plasma and 100 μL of acetonitrile. The plate was sealed and vortexed (1,650 rpm, 3 min), and subsequently centrifuged (3,500 rpm, 10 min) at room temperature. Fifty microliters of supernatant was transferred to a separate 96-well collection plate containing 50 μL water per well. The plate was vortexed (1,600 rpm, 1 min) and samples were injected into the LC-MS-tandem MS system for analysis.

The separation column was a Zorbax SB-Phenyl, 1.7 μm, 40 × 2.1 mm column (Agilent). The mobile phase was water containing 0.1% formic acid (mobile phase A) and methanol containing 0.1% formic acid (mobile phase B). The flow rate was 0.8 mL min^{-1} with an operating column temperature of 50°C. The gradient was from 25% to 80% B in 1 min, then 80%–98% B in 0.7 min followed by a 1 min hold, then 98%–80% B in 0.7 min followed by a 0.5 min hold, and finally brought back to 25% B in 0.5 min followed by 1.35 min of re-equilibration.

The MS instrument was operated in multiple reaction monitoring (MRM) mode and positive electrospray ion mode with the following ion source conditions: curtain gas, 35 psi; gas 1, 70 psi; gas 2, 80 psi; ion spray voltage, 5,500 V; and temperature, 500°C. The MRM transition and collision energy were m/z 936.6 > 409.3 and 74 V for RPM, m/z 826.6 > 616.4 and 48 V for TAC, and m/z 271.0 > 155.1 and 25 V for the internal standard, tolbutamide.

T cell generation, base editing, and lentiviral transduction

Healthy donor adult human leukopaks were obtained from HemaCare (Charles River). T cells were isolated using StraightFrom Leukopak CD4/CD8 MicroBead Kit (Miltenyi Biotec) following the manufacturer's protocol and cryopreserved in CS10 (STEMCELL Technologies). Syngeneic HIS mouse-derived T cells were isolated from splenic tissue of a reconstituted huNCG mouse using CD2 Microbeads (Miltenyi Biotec) following the manufacturer's protocol and cryopreserved in CS10. T cells were thawed and placed in culture at 10^6 cells mL^{-1} in complete medium comprising ImmunoCult XF T

Cell Expansion Medium (STEMCELL Technologies), 1% penicillin-streptomycin, 2 mM GlutaMax, 25 mM HEPES Buffer (Life Technologies), and 5% CTS ImmuneCell SR (Thermo Fisher). Complete medium was complemented with 10 ng mL^{-1} human IL-15 (BioLegend) and 10 ng mL^{-1} IL-7 (BioLegend). T cells were stimulated with ImmunoCult Human CD3/CD28/CD2 T cell activator (STEMCELL Technologies) following the manufacturer's instructions and incubated at 37°C, 5% CO_2, and 95% humidity. Two days post-activation, T cells were counted, washed with sterile PBS, and resuspended in P3 buffer (Lonza) at 5×10^7 cells mL^{-1}. T cells were electroporated with 1 μg sgRNA from Agilent and 2 μg mRNA encoding ABE8.20m or BE4 per 10^6 cells using the Lonza 4D Nucleofector system (program DH-102). Base editing with more than 1 sgRNA was achieved by adding 1 μg of the additional sgRNA(s) per 10^6 cells to the electroporation reaction. T cells then recovered in complete medium at 10^6 cells mL^{-1} and were transduced with 300 μL of concentrated lentiviral vector supernatant per 10^6 cells. Medium was exchanged every other day to adjust cell concentration to 5×10^5 cells mL^{-1} until day 10 when cells were cryopreserved in CS10. Sequences for the 20 nucleotide protospacers for *CD3E*, *TRAC*, *B2M*, *CIITA*, and *FKBP1A* can be found in Table S1. T cell products for *in vivo* studies were generated using *TRAC* sgRNA and BE4 mRNA (Figure S1); *TRAC*, *B2M* (TSBTx845), *CIITA* sgRNAs, and BE4 mRNA (Figures 1F–1I); *CD3E*, *B2M* (TSBTx760), *CIITA* sgRNAs, and ABE8.20m mRNA (Figures 1L–1N and 3); *FKBP1A* (TSBTx1538) sgRNA and ABE8.20m mRNA (Figure 5); and *CD3E*, *B2M*, *CIITA, FKBP1A* sgRNAs, and ABE8.20m mRNA (Figure 6). All T cell products for *in vitro* assays were generating using *B2M*, *CIITA, FKBP1A* sgRNAs, and ABE8.20m mRNA.

Plasmid construction

The transgene cassette comprising a CD4-based CAR and molecular tag comprising GFP or truncated NGFR, EGFR, or CD19 separated by an intervening T2A linker is described elsewhere.[78,79] The CD19-specific CAR comprised the FMC63 single-chain variable fragment,[80] CD8α hinge/transmembrane domain, and 4-1BB/CD3ζ intracellular domain, and was separated by a T2A linker to truncated EGFR. To generate the NFAT-GFP reporter plasmid, six NFAT response elements (GGAGGAAAAACTGTTTC ATACAGAAGGCGT) were cloned upstream of the murine IFN-β promoter driving expression of GFP. The HLA single-chain molecules were cloned into an expression cassette upstream of a T2A linker and truncated EGFR. HLA single-chain molecules are fusion proteins consisting of B2M signal peptide, B2M mature chain, $(G_4S)_3$ linker, and the HLA extracellular, transmembrane, and cytoplasmic domains. HLA alleles include HLA-Bw4 group: HLA-B*57:01; HLA-C1 group: HLA-C*01:02 and C*07:02; HLA-C2 group: HLA-C*04:01, C*05:01, C*06:02, and C*18:01; and HLA-E*01:03. HLA-E single chain comprised an HLA-G*01 signal sequence-derived peptide (VMAPRTLFL) between the signal peptide and B2M chain. HLA amino acid sequences are from the IPD-IMGT/HLA database. All gene fragments were codon optimized (IDT), and then custom synthesized and cloned by GenScript into a self-inactivating (SIN) lentiviral vector.

Lentivirus production

Lentiviral particles were generated using packaging expression vectors from Aldevron: VSV glycoprotein (pALD-VSV-G), HIV Rev (pALD-Rev), and HIV Gag/Pol (pALD-GagPol). The packaging plasmids and the appropriate SIN transfer vector were transfected into HEK293T cells using Lipofectamine 2000 (Life Technologies). At 24 h post-transfection, the supernatant was collected, filtered through a 0.45-μm syringe-driven filter, mixed with PEG-it Virus Precipitation Solution (System Biosciences) and stored at 4°C overnight following the manufacturer's instructions. After incubation, the virus solution was concentrated by centrifugation for 30 min at 1,500 × *g*, 4°C. The supernatant was aspirated, and the virus pellet was resuspended in 600 μL of complete medium and stored at −80°C.

Next-generation sequencing of genomic DNA

Genomic DNA (gDNA) samples were prepared to determine base editing efficiency as described previously.[81] In brief, 5×10^5 cells were lysed using QuickExtract DNA Extraction Solution (Lucigen) according to the manufacturer's protocol. Two microliters of gDNA was added to a 25 μL polymerase chain reaction (PCR) containing Q5 High-Fidelity DNA Polymerase (New England Biolabs) and 0.5 μM forward and reverse primers. Primer sequences for gDNA amplification are listed in Table S1. PCR products were then amplified using unique Illumina barcoding primer pairs, and then the resulting product was purified using solid-phase reversible immobilization beads (Beckman Coulter) and quantified using a NanoDrop 1000 Spectrophotometer (Thermo Fisher Scientific). Barcoded amplicons were sequenced on an Illumina MiSeq instrument according to the manufacturer's instructions.

Base editor mRNA production

mRNA production for adenosine (ABE8.20m)[82] and cytosine (BE4)[81] base editors was performed as described previously. In brief, editors were cloned into a plasmid comprising a T7 promoter, 5′ UTR, Kozak sequence, open reading frame encoding the editor, 3′ UTR, and poly(A) tail. Plasmids were linearized using BbsI-HF (New England Biolabs) and purified using DNA Clean and Concentrate Columns (Zymo Research). Linearized plasmid served as template for *in vitro* transcription with HiScribe T7 High-Yield RNA Synthesis Kit (New England BioLabs) following the manufacturer's instructions, except CleanCap AG (TriLink Biotechnologies) was used for cotranscriptional capping. mRNA was purified using lithium chloride precipitation.

Tumor cell line generation

JeKo-1 (CRL-3006), Raji (CCL-86), and Nalm6, clone G5 (CRL-3273), were obtained from the ATCC. Cell lines were transduced with a lentiviral vector encoding both GFP and Click Beetle Green luciferase (Luc). Nalm6 cells were also transduced with a lentiviral vector encoding iRFP670. To generate JeKo-1.*FKBP1A*^{KO}.Luc cells, parental JeKo-1.Luc cells were electroporated with 1 μg TSBTx1538 sgRNA and 2 μg ABE8.20m mRNA using the Lonza 4D Nucleofector system (SF buffer, program DJ-105). To generate

Nalm6.CD19^{KO}.iRFP670 cells, parental Nalm6.iRFP670 cells were electroporated with 1 μg TSBTx3773 sgRNA and 2 μg ABE8.20m mRNA using the Lonza 4D Nucleofector system (SF buffer, program CV-104). All tumor cells were sorted on GFP or iRFP670 positivity, or CD19-negative surface expression using the Aria Phusion (BD Bioscience) to obtain a clonal population. Single cell clones were analyzed by next-generation sequencing to confirm *FKBP1A* disruption.

Mixed leukocyte reaction

Alloreactive T cells were generated in Figures 1D and 1E by culturing HLA-A*02^{-} CD3^{+} T cells (effectors) with HLA-A*02^{+} CD3-depleted PBMCs (targets) from a separate donor in duplicate. CD3 selections were performed using CD3 MicroBeads (Miltenyi Biotec) following the manufacturer's protocol. Effector and target cells were mixed at a 1:1 ratio in complete medium supplemented with 300 U mL^{-1} IL-2 (Sartorius) for 7–10 days. Activated HLA-A*02^{-} effector T cells were then cultured at different ratios with PBMC donor-matched HLA-A*02^{+} T cells that were unmodified HLA-A*02^{+} (on-target) or HLA-deficient *B2M*^{KO}*CIITA*^{KO} (off-target) and labeled with CellTrace Far Red (Thermo Fisher Scientific). On- and off-target T cells were combined at 1:1 ratio before adding effector T cells to measure the relative frequency of target T cells within the same well 48 h post-culture using flow cytometry.

For the study described in Figure S7, CellTrace Violet (Thermo Fisher Scientific) CD3^{+} T cells (effectors) and CD3-depleted PBMCs (targets) from HLA-mismatched donors were cultured in triplicate at a 1:1 ratio in complete medium supplemented with 300 U mL^{-1} IL-2. Cells were cultured in the presence of RPM at 10^{-2}, 10^{-3}, and 10^{-4} μg mL^{-1}, TAC at 10^{0}, 10^{-1}, and 10^{-2} μg mL^{-1}, and DMSO VEH control. Effector T cells cultured in the absence of target cells served as an unstimulated control. Frequency of dividing effector CD8^{+} and CD4^{+} T cells was measured at 5 and 7 days post-stimulation by flow cytometry.

NK cell cytotoxicity and degranulation assays

Human NK cells were isolated using StraightFrom Leukopak REAlease CD56 MicroBead Kit (Miltenyi Biotec) or CD56 MicroBeads (Miltenyi Biotec). NK cells were primed for 3 days in complete medium with 5 ng mL^{-1} IL-15 and 300 U mL^{-1} IL-2. Primed NK cells were then cultured at different ratios with allogeneic T cells that were unmodified HLA^{+} (off-target) or HLA-deficient *B2M*^{KO}*CIITA*^{KO} (on-target). On- and off-target T cells were combined at a 1:1 ratio before adding NK cells to measure the relative change in frequency of target T cells compared with control wells in the absence of NK cells. Specific lysis of on-target T cells was measured 48 h post-culture by flow cytometry using the formula: specific lysis (%) = 100 – (100 × (% survival in the presence of NK cells/% survival in the absence of NK cells)). NK cell degranulation was measured by culturing 10^{5} primed NK cells with 10^{5} on-target or off-target allogeneic T cells, or alone. Anti-CD107a antibody was added at the start of stimulation followed by the addition of 1X Monensin Solution and 1X Brefeldin A (BioLegend) 1 h later. Cells were incubated for 6 h total before analysis by flow cytometry.

CAR-T cell cytotoxicity assays

Cryopreserved UTD T cells, unmodified 19CAR-T cells, and *FKBP1A*^{KO} 19CAR-T cells were thawed and rested overnight at 37°C, 5% CO_2. To perform the Incucyte cytotoxicity assay, a 96-well flat-bottom plate (Corning) was coated with 0.01% poly-L-ornithine solution (Sigma-Aldrich) for 30 min, and then decanted and left to dry for 30 min. Afterward, 2.5 × 10^{4} JeKo-1.*FKBP1A*^{KO}.GFP^{+} tumor cells were seeded into the 96-well plate and cultured in triplicate with rested T cells at 0:1, 1:1, 0.25:1, and 0.125:1 effector-to-target cell (E/T) ratios. RPM (100 nM), TAC (100 ng mL^{-1}), and VEH (DMSO) control were added at the start of culture and then again at 48, 96, and 144 h post-culture. Samples were transferred to an Incucyte SX5 Live-Cell Analysis System (Sartorius) and imaged every 4 h to assess GFP fluorescence intensity.

To perform the VITAL cytotoxicity assay,[83] 2.5 × 10^{4} Nalm6.CD19^{WT}.GFP^{+} cells and 2.5 × 10^{4} Nalm6.CD19^{KO}.iRFP670^{+} cells were seeded per well of a 96-well flat-bottom plate. UTD T cells, unmodified 19CAR-T cells, and *FKBP1A*^{KO} 19CAR-T cells were added at 0:125:1, 0.06:1, 0.03:1, 0.015:1, and 0:1 E/T ratios. RPM (100 nM), TAC (100 ng mL^{-1}), and VEH (DMSO) control were added at the start of culture. Samples were incubated at 37°C, 5% CO_2 for 48 h before flow cytometric analysis to measure the frequency of viable GFP^{+} and iRFP670^{+} Nalm6 tumor cells. Specific lysis of Nalm6.GFP^{+} cells was measured using the formula: specific lysis (%) = 100 – (100 × (% survival in the presence of T cells/% survival in the absence of T cells)).

CAR-T cell cytokine production assay

Cryopreserved unmodified and *FKBP1A*^{KO} 19CAR-T cells were thawed into complete medium and rested overnight at 10^{6} cells mL^{-1} in the incubator at 37°C, 5% CO_2. T cells were pretreated overnight with RPM (100 nM), TAC (100 ng mL^{-1}), dexamethasone (10 μg mL^{-1}; Sigma-Aldrich), prednisone (1 μg mL^{-1}; Sigma-Aldrich), or VEH (DMSO) control prior to assay set-up. The following day, T cells were washed, counted and 10^{5} cells were seeded in duplicate into a 96-well flat-bottom plate alone or with 10^{5} JeKo-1.GFP^{+} tumor cells in the presence of drug treatments. Anti-CD107a antibody was added at the start of stimulation followed by the addition of 1X Monensin Solution and 1X Brefeldin A (BioLegend) 1 h later. Cells were incubated for 6 h total before analysis by flow cytometry.

CAR-T cell and tumor proliferation assays

Cryopreserved unmodified and *FKBP1A*^{KO} 19CAR-T cells were thawed into complete medium and rested overnight at 10^{6} cells mL^{-1} in the incubator at 37°C, 5% CO_2. The following day, T cells were washed, counted, and 10^{4} cells were seeded in triplicate into a 96-well flat-bottom plate alone or with 10^{4} JeKo-1.GFP^{+}

tumor cells. Complete medium was supplemented with RPM (100 nM), TAC (100 ng mL^{-1}), dexamethasone (10 μg mL^{-1}), prednisone (1 μg mL^{-1}), or VEH (DMSO) control and refreshed on days 2, 4, and 6 post-culture. On day 7, samples were analyzed by flow cytometry and 19CAR-T cells were enumerated using CountBright Counting Beads (Thermo Fisher Scientific) following the manufacturer's protocol.

Raji, Nalm6, and JeKo-1 tumor cells were cultured in complete R10 medium comprising RPMI 1640 Medium (Thermo Fisher Scientific) supplemented with 10% fetal bovine serum, 1% penicillin-streptomycin, 2 mM GlutaMax, and 25 mM HEPES buffer (Life Technologies) at 2.5×10^4 cells mL^{-1} and seeded into a 24-well tissue culture plate. Tumor cells were plated in triplicate per treatment condition. RPM was added at 10 and 0.1 μg mL^{-1}, and DMSO served as VEH control. Cells were incubated at 37°C, 5% CO_2, and viable cell counts were determined using the NucleoCounter NC200 (ChemoMetec) at 2 and 4 days post-culture.

Flow cytometry

Cultured cells were washed and stained in 50 μL of 1X PBS containing 2 mM EDTA and 2% fetal calf serum, and whole blood was stained directly with anti-human antibodies from BioLegend: CD45 (HI30), CD3 (OKT3), CD2 (RPA-2.10), CD4 (OKT4), CD8 (SK1), CD56 (5.1H11), CD107a (H4A3), CD19 (HIB19), CD22 (HIB22), HLA-A2 (BB7.2), HLA-DR (L243), NGFR (ME20.4), EGFR (AY13), NKG2A (S19004C), LIR-1 (GHI/75), HLA-ABC (W6/32), KIR2DL1 (HP-DM1), KIR2DL2/L3 (DX27), KIR3DL1 (DX9), KIR2DL4 (mAB33), and KIR2DL5 (UP-R1). Live cells were discriminated by staining negative for Fixable Viability Dye eFluor780 (eBioscience). CountBright Counting Beads were used according to the manufacturer's instructions to determine the cell concentration from whole blood and tissue. Intracellular cytokines were detected using Cell Fixation & Cell Permeability Kit (Invitrogen) following the manufacturer's protocol with anti-human antibodies from BioLegend: TNF-α (MAb11), IFN-γ (4S.B3), IL-2 (MQH-17H12), and GM-CSF (BVD2-21C11). Phosphorylated intracellular proteins were detected using BD Cytofix Fixation Buffer and BD Phosflow Perm Buffer III (BD Biosciences) according to the manufacturer's instructions with anti-human antibodies from BD Biosciences: mTOR-pS2448 (O21-404), S6-pS235/pS236 (N7-548), and 4EBP1-pT36/pT45 (M31-16). Flow cytometry data were acquired on the MACSQuant Analyzer 16 (Miltenyi Biotec) and FACSymphony A3 Cell Analyzer (BD Biosciences). Data were analyzed using FlowJo software v.10 (Tree Star).

mTOR and calcineurin downstream assays

To evaluate downstream mTOR activity in T cells, phosphorylation of S6 was detected by incubating 2×10^5 T cells overnight in complete medium supplemented with RPM (1 nM) or DMSO VEH control at 37°C, 5% CO_2. Subsequently, T cells were washed and stained with Fixable Viability Dye eFlour780 according to the manufacturer's protocol. T cells were then seeded into a 96-well flat-bottom plate with RPM (1 nM) or DMSO and stimulated with Immunocult T cell Activator (1:40 dilution) or unstimulated for 1 h at 37°C, 5% CO_2, prior to analysis by flow cytometry. To detect calcineurin activity in T cells, 2×10^5 T cells expressing an NFAT-GFP reporter were cultured in complete medium supplemented with TAC (100 ng mL^{-1}) or DMSO VEH control. T cells were then stimulated using an Immunocult T Cell Activator (1:40 dilution) or unstimulated and cultured overnight at 37°C, 5% CO_2, prior to analysis by flow cytometry. For both assays, T cells were unmodified or base edited to disrupt *FKBP1A*. To evaluate mTOR activity in B cell tumor lines, phosphorylation of mTOR, S6, and 4EBP1 was detected by incubating 1×10^5 Raji, Nalm6, and JeKo-1 cells overnight in R10 medium in a 96-well flat-bottom plate at 37°C, 5% CO_2. Tumor cells were treated with either RPM (10 mg mL^{-1}) or DMSO VEH control. The following day, tumor cells were prepared for flow cytometric analysis.

Protein detection

Unmodified and $FKBP1A^{KO}$ T cells ($1–5 \times 10^6$) were washed with PBS and lysates were prepared using cold RIPA Buffer (Thermo Fisher Scientific) with Halt Protease and Phosphatase Inhibitor Cocktail (Thermo Fisher Scientific) according to the manufacturer's protocol. Supernatants were collected and stored at −80°C. Protein was quantified using Pierce 660nm Protein Assay Reagent (Thermo Fisher Scientific) following the manufacturer's instructions. Detection and quantification of FKBP1A and GAPDH control was determined using ProteinSimple Jess (Biotechne). In brief, protein samples were diluted to 0.5 mg mL^{-1} using Sample Buffer, combined with Fluorescent Master Mix from EZ Standard Pack 5 (Biotechne), and then denatured at 95°C, 5 min. For FKBP1A protein detection, rabbit anti-human FKBP12 monoclonal antibody (Abcam) was diluted 1:100 in antibody diluent, combined with anti-rabbit secondary HRP antibody, chemiluminescent substrate, and peroxide from Biotechne. For GAPDH protein detection, mouse anti-human GAPDH monoclonal antibody (Cell Signaling Technologies) was diluted 1:100 in antibody diluent and combined with anti-mouse secondary NIR (Biotechne). All samples including the 2–40 kDa separation module (Biotechne) were loaded onto the capillary cartridge (Biotechne) according to the instructions. The plate was analyzed on the Jess, where chemiluminescence measured FKBP1A and fluorescence measured GAPDH. ProteinSimple Compass for SW software was used to quantify area under the curve for total protein signal.

Statistical analysis

Comparison of matched samples were performed using two-sided non-parametric Wilcoxon matched pairs signed rank test. Comparison of unmatched samples were performed using two-sided Student's t test, non-parametric Wilcoxon rank-sum test, or Kruskal-Wallace test followed by Dunn's test for multiple comparisons. Bivariate correlations were performed using two-sided Spearman's rank correlation. Area under the curve calculations were performed using either cell concentration per microliter of blood or frequency of cells. All statistical analyses were performed using GraphPad Prism version 9.3.0 (GraphPad).

DATA AND CODE AVAILABILITY

Plasmids encoding ABE8.20m and BE4 base editors used in this work are available from Addgene. The 20 nucleotide protospacer sequences and primers for the amplification of on-target amplicons can be found in Table S1. Amino acid sequences of HLA alleles used in this work are available from the IPD-IMGT/HLA database (https://www.ebi.ac.uk/ipd/imgt/hla/).

SUPPLEMENTAL INFORMATION

Supplemental information can be found online at https://doi.org/10.1016/j.ymthe.2024.06.022.

ACKNOWLEDGMENTS

We thank J. Decker, A. Cozier, M. Patel, C. Lazzara, L. Young, and L. Barrera for next-generation sequencing and computational support. We acknowledge L. Hardy and H. Kromer for single-cell sorting, and W. Schmidt, N. Mastrangelo, J. Bynoe, and E. Chiang for facilitating institutional interactions between Beam Therapeutics and the Ragon Institute. This study was supported by internal funding from Beam Therapeutics and NIH grant R37 AI170189 (to T.M.A). BioRender.com was used to create some figures.

AUTHOR CONTRIBUTIONS

C.R.M. conceived and directed the work, designed and conducted experiments, performed analyses, and wrote the manuscript. A.C.M. and P.B.B. designed and conducted *in vitro* experiments to interrogate *FKBP1A* disruption in CAR-T cells and performed analyses. L.J.C. performed the huNK mouse study and NK cell phenotyping, and C.K. generated lentivirus and T cells for *in vitro* and *in vivo* experiments. A.J.C. and D.T.C. designed and supervised *in vivo* experiments, and F.M.M., M.L.W., J.J.R., V.D.V., and E.M. carried out all animal studies. F.L. and B.Y. were responsible for mass spectrometry and analysis. T.M.A. oversaw research. C.R.M., A.J.C., D.T.C., C.L.B., and T.M.A. edited the manuscript.

DECLARATION OF INTERESTS

C.R.M., A.C.M., P.B.B., A.J.C., F.M.M., M.L.W., J.J.R., L.J.C., C.K., F.L., and B.Y. were employees of Beam Therapeutics when the work was conducted and are shareholders in the company. Beam Therapeutics has filed patent applications based on this work.

REFERENCES

1. Wang, X., Borquez-Ojeda, O., Stefanski, J., Du, F., Qu, J., Chaudhari, J., Thummar, K., Zhu, M., Shen, L.B., Hall, M., et al. (2021). Depletion of high-content CD14+ cells from apheresis products is critical for successful transduction and expansion of CAR T cells during large-scale cGMP manufacturing. Mol. Ther. Methods Clin. Dev. *22*, 377–387. https://doi.org/10.1016/j.omtm.2021.06.014.

2. Allen, E.S., Stroncek, D.F., Ren, J., Eder, A.F., West, K.A., Fry, T.J., Lee, D.W., Mackall, C.L., and Conry-Cantilena, C. (2017). Autologous lymphapheresis for the production of chimeric antigen receptor T cells. Transfusion (Paris) *57*, 1133–1141. https://doi.org/10.1111/trf.14003.

3. Depil, S., Duchateau, P., Grupp, S.A., Mufti, G., and Poirot, L. (2020). Off-the-shelf' allogeneic CAR T cells: development and challenges. Nat. Rev. Drug Discov. *19*, 185–199. https://doi.org/10.1038/s41573-019-0051-2.

4. Kernan, N.A., Collins, N.H., Juliano, L., Cartagena, T., Dupont, B., and O'Reilly, R.J. (1986). Clonable T lymphocytes in T cell-depleted bone marrow transplants correlate with development of graft-v-host disease. Blood *68*, 770–773. https://doi.org/10.1182/blood.v68.3.770.bloodjournal683770.

5. Qasim, W., Zhan, H., Samarasinghe, S., Adams, S., Amrolia, P., Stafford, S., Butler, K., Rivat, C., Wright, G., Somana, K., et al. (2017). Molecular remission of infant B-ALL after infusion of universal TALEN gene-edited CAR T cells. Sci. Transl. Med. *9*, eaaj2013. https://doi.org/10.1126/scitranslmed.aaj2013.

6. Philip, L.P.B., Schiffer-Mannioui, C., Le Clerre, D., Chion-Sotinel, I., Derniame, S., Potrel, P., Bas, C., Lemaire, L., Galetto, R., Lebuhotel, C., et al. (2015). Multiplex genome-edited T-cell manufacturing platform for "off-the-shelf" adoptive T-cell immunotherapies. Cancer Res. *75*, 3853–3864. https://doi.org/10.1158/0008-5472.CAN-14-3321.

7. Anasetti, C., Amos, D., Beatty, P.G., Appelbaum, F.R., Bensinger, W., Buckner, C.D., Clift, R., Doney, K., Martin, P.J., Mickelson, E., et al. (1989). Effect of HLA Compatibility on Engraftment of Bone Marrow Transplants in Patients with Leukemia or Lymphoma. N. Engl. J. Med. *320*, 197–204. https://doi.org/10.1056/nejm198901263200401.

8. Kagoya, Y., Guo, T., Yeung, B., Saso, K., Anczurowski, M., Wang, C.H., Murata, K., Sugata, K., Saijo, H., Matsunaga, Y., et al. (2020). Genetic ablation of HLA class I, class II, and the T-cell receptor enables allogeneic T cells to be used for adoptive T-cell therapy. Cancer Immunol. Res. *8*, 926–936. https://doi.org/10.1158/2326-6066.CIR-18-0508.

9. Lee, J., Sheen, J.H., Lim, O., Lee, Y., Ryu, J., Shin, D., Kim, Y.Y., and Kim, M. (2020). Abrogation of HLA surface expression using CRISPR/Cas9 genome editing: a step toward universal T cell therapy. Sci. Rep. *10*, 17753. https://doi.org/10.1038/s41598-020-74772-9.

10. Kärre, K., Ljunggren, H.G., Piontek, G., and Kiessling, R. (1986). Selective rejection of H-2-deficient lymphoma variants suggests alternative immune defence strategy. Nature *319*, 675–678. https://doi.org/10.1038/319675a0.

11. Moes, D.J.A., Guchelaar, H.J., and De Fijter, J.W. (2015). Sirolimus and everolimus in kidney transplantation. Drug Discov. Today *20*, 1243–1249. https://doi.org/10.1016/j.drudis.2015.05.006.

12. Reichenspurner, H. (2005). Overview of tacrolimus-based immunosuppression after heart or lung transplantation. J. Heart Lung Transpl. *24*, 119–130. https://doi.org/10.1016/j.healun.2004.02.022.

13. Sharma, N., Zhao, Q., Ni, B., Elder, P., Puto, M., Benson, D.M., Rosko, A., Chaudhry, M., Devarakonda, S., Bumma, N., et al. (2021). Effect of early post-transplantation tacrolimus concentration on the risk of acute graft-versus-host disease in allogenic stem cell transplantation. Cancers (Basel) *13*, 613. https://doi.org/10.3390/cancers13040613.

14. Chen, X., Sun, H., Cassady, K., Yang, S., Chen, T., Wang, L., Yan, H., Zhang, X., and Feng, Y. (2021). The Addition of Sirolimus to GVHD Prophylaxis After Allogeneic Hematopoietic Stem Cell Transplantation: A Meta-Analysis of Efficacy and Safety. Front. Oncol. *11*. https://doi.org/10.3389/fonc.2021.683263.

15. Schreiber, S.L. (1991). Chemistry and Biology of the Immunophilins and Their Immunosuppressive Ligands. Science *251*, 283–287. https://doi.org/10.1126/science.1702904.

16. Chen, Y., Chen, H., Rhoad, A.E., Warner, L., Caggiano, T.J., Failli, A., Zhang, H., Hsiao, C.L., Nakanishi, K., and Molnar-Kimber, K.L. (1994). A putative sirolimus (rapamycin) effector protein. Biochem. Biophys. Res. Commun. *203*, 1–7. https://doi.org/10.1006/bbrc.1994.2140.

17. Brown, E.J., Albers, M.W., Shin, T.B., Ichikawa, K., Keith, C.T., Lane, W.S., and Schreiber, S.L. (1994). A mammalian protein targeted by G1-arresting rapamycin-receptor complex. Nature *369*, 756–758. https://doi.org/10.1038/369756a0.

18. Sabers, C.J., Martin, M.M., Brunn, G.J., Williams, J.M., Dumont, F.J., Wiederrecht, G., and Abraham, R.T. (1995). Isolation of a protein target of the FKBP12-rapamycin complex in mammalian cells. J. Biol. Chem. *270*, 815–822. https://doi.org/10.1074/jbc.270.2.815.

19. Mattila, P.S., Ullman, K.S., Fiering, S., Emmel, E.A., McCutcheon, M., Crabtree, G.R., and Herzenberg, L.A. (1990). The actions of cyclosporin A and FK506 suggest a novel step in the activation of T lymphocytes. EMBO J. *9*, 4425–4433. https://doi.org/10.1002/j.1460-2075.1990.tb07893.x.

20. Terada, N., Lucas, J.J., Szepesi, A., Franklin, R.A., Domenico, J., and Gelfand, E.W. (1993). Rapamycin blocks cell cycle progression of activated T cells prior to events

characteristic of the middle to late G1 phase of the cycle. J. Cell. Physiol. *154*, 7–15. https://doi.org/10.1002/jcp.1041540103.

21. Dumont, F.J., Staruch, M.J., Koprak, S.L., Melino, M.R., and Sigal, N.H. (1990). Distinct mechanisms of suppression of murine T cell activation by the related macrolides FK-506 and rapamycin. J. Immunol. *144*, 251–258. https://doi.org/10.4049/jimmunol.144.1.251.

22. Tocci, M.J., Matkovich, D.A., Collier, K.A., Kwok, P., Dumont, F., Lin, S., Degudicibus, S., Siekierka, J.J., Chin, J., and Hutchinson, N.I. (1989). The immunosuppressant FK506 selectively inhibits expression of early T cell activation genes. J. Immunol. *143*, 718–726. https://doi.org/10.4049/jimmunol.143.2.718.

23. Kino, T., Hatanaka, H., Miyata, S., Inamura, N., Nishiyama, M., Yajima, T., Goto, T., Okuhara, M., Kohsaka, M., Aoki, H., et al. (1987). Fk-506, A Novel Immunosuppressant Isolated From A Streptomyces Ii. Immunosuppressive Effect Of Fk-506 In Vitro. J. Antibiot. *40*, 1256–1265. https://doi.org/10.7164/antibiotics.40.1256.

24. Rong, Z., Wang, M., Hu, Z., Stradner, M., Zhu, S., Kong, H., Yi, H., Goldrath, A., Yang, Y.G., Xu, Y., and Fu, X. (2014). An effective approach to prevent immune rejection of human ESC-derived allografts. Cell Stem Cell *14*, 121–130. https://doi.org/10.1016/j.stem.2013.11.014.

25. Xiao, F., Ma, L., Zhao, M., Huang, G., Mirenda, V., Dorling, A., Lechler, R., and Lombardi, G. (2014). Ex vivo expanded human regulatory T cells delay islet allograft rejection via inhibiting islet-derived monocyte chemoattractant protein-1 production in CD34+ stem cells-reconstituted NOD-scid IL2rγnull mice. PLoS One *9*, e90387. https://doi.org/10.1371/journal.pone.0090387.

26. Huntington, N.D., Legrand, N., Alves, N.L., Jaron, B., Weijer, K., Plet, A., Corcuff, E., Mortier, E., Jacques, Y., Spits, H., and Di Santo, J.P. (2009). IL-15 trans-presentation promotes human NK cell development and differentiation in vivo. J. Exp. Med. *206*, 25–34. https://doi.org/10.1084/jem.20082013.

27. Kaur, K., and Jewett, A. (2022). Differences in Tumor Growth and Differentiation in NSG and Humanized-BLT Mice; Analysis of Human vs. Humanized-BLT-Derived NK Expansion and Functions. Cancers (Basel) *15*, 112. https://doi.org/10.3390/cancers15010112.

28. Kalberer, C.P., Siegler, U., and Wodnar-Filipowicz, A. (2003). Human NK cell development in NOD/SCID mice receiving grafts of cord blood CD34+ cells. Blood *102*, 127–135. https://doi.org/10.1182/blood-2002-07-2024.

29. Katano, I., Nishime, C., Ito, R., Kamisako, T., Mizusawa, T., Ka, Y., Ogura, T., Suemizu, H., Kawakami, Y., Ito, M., and Takahashi, T. (2017). Long-term maintenance of peripheral blood derived human NK cells in a novel human IL-15- transgenic NOG mouse. Sci. Rep. *7*, 17230. https://doi.org/10.1038/s41598-017-17442-7.

30. Guo, Y., Xu, B., Wu, Z., Bo, J., Tong, C., Chen, D., Wang, J., Wang, H., Wang, Y., and Han, W. (2021). Mutant B2M-HLA-E and B2M-HLA-G fusion proteins protects universal chimeric antigen receptor-modified T cells from allogeneic NK cell-mediated lysis. Eur. J. Immunol. *51*, 2513–2521. https://doi.org/10.1002/eji.202049107.

31. Li, W., Zhu, X., Xu, Y., Chen, J., Zhang, H., Yang, Z., Qi, Y., Hong, J., Li, Y., Wang, G., et al. (2022). Simultaneous editing of TCR, HLA-I/II and HLA-E resulted in enhanced universal CAR-T resistance to allo-rejection. Front. Immunol. *13*, 1052717. https://doi.org/10.3389/fimmu.2022.1052717.

32. Jo, S., Das, S., Williams, A., Chretien, A.S., Pagliardini, T., Le Roy, A., Fernandez, J.P., Le Clerre, D., Jahangiri, B., Chion-Sotinel, I., et al. (2022). Endowing universal CAR T-cell with immune-evasive properties using TALEN-gene editing. Nat. Commun. *13*, 3453. https://doi.org/10.1038/s41467-022-30896-2.

33. Torikai, H., Mi, T., Gragert, L., Maiers, M., Najjar, A., Ang, S., Maiti, S., Dai, J., Switzer, K.C., Huls, H., et al. (2016). Genetic editing of HLA expression in hematopoietic stem cells to broaden their human application. Sci. Rep. *6*, 21757. https://doi.org/10.1038/srep21757.

34. Xu, H., Wang, B., Ono, M., Kagita, A., Fujii, K., Sasakawa, N., Ueda, T., Gee, P., Nishikawa, M., Nomura, M., et al. (2019). Targeted Disruption of HLA Genes via CRISPR-Cas9 Generates iPSCs with Enhanced Immune Compatibility. Cell Stem Cell *24*, 566–578.e7. https://doi.org/10.1016/j.stem.2019.02.005.

35. Purdy, A.K., and Campbell, K.S. (2009). Natural killer cells and cancer: Regulation by the killer cell ig-like receptors (KIR). Cancer Biol. Ther. *8*, 2211–2220. https://doi.org/10.4161/cbt.8.23.10455.

36. Ichise, H., Nagano, S., Maeda, T., Miyazaki, M., Miyazaki, Y., Kojima, H., Yawata, N., Yawata, M., Tanaka, H., Saji, H., et al. (2017). NK Cell Alloreactivity against KIR-Ligand-Mismatched HLA-Haploidentical Tissue Derived from HLA Haplotype-Homozygous iPSCs. Stem Cell Rep. *9*, 853–867. https://doi.org/10.1016/j.stemcr.2017.07.020.

37. Neelapu, S.S., Locke, F.L., Bartlett, N.L., Lekakis, L.J., Miklos, D.B., Jacobson, C.A., Braunschweig, I., Oluwole, O.O., Siddiqi, T., Lin, Y., et al. (2017). Axicabtagene Ciloleucel CAR T-Cell Therapy in Refractory Large B-Cell Lymphoma. N. Engl. J. Med. *377*, 2531–2544. https://doi.org/10.1056/nejmoa1707447.

38. Liu, S., Deng, B., Yin, Z., Pan, J., Lin, Y., Ling, Z., Wu, T., Chen, D., Chang, A.H., Gao, Z., et al. (2020). Corticosteroids do not influence the efficacy and kinetics of CAR-T cells for B-cell acute lymphoblastic leukemia. Blood Cancer J. *10*, 15. https://doi.org/10.1038/s41408-020-0280-y.

39. Lakomy, T., Akhoundova, D., Nilius, H., Kronig, M.N., Novak, U., Daskalakis, M., Bacher, U., and Pabst, T. (2023). Early Use of Corticosteroids following CAR T-Cell Therapy Correlates with Reduced Risk of High-Grade CRS without Negative Impact on Neurotoxicity or Treatment Outcome. Biomolecules *13*, 382. https://doi.org/10.3390/biom13020382.

40. Sebestyén, A., Sticz, T.B., Márk, Á., Hajdu, M., Timár, B., Nemes, K., Nagy, N., Váradi, Z., and Kopper, L. (2012). Activity and complexes of mTOR in diffuse large B-cell lymphomas - A tissue microarray study. Mod. Pathol. *25*, 1623–1628. https://doi.org/10.1038/modpathol.2012.141.

41. Vajpayee, N., Thakral, C., Gopaluni, S., Newman, N., and Gajra, A. (2012). Activation of mammalian target of rapamycin in diffuse large B-cell lymphoma: A clinicopathological study. Leuk. Res. *36*, 1403–1409. https://doi.org/10.1016/j.leukres.2012.07.016.

42. Gottschalk, A.R., Boise, L.H., Thompson, C.B., and Quintáns, J. (1994). Identification of immunosuppressant-induced apoptosis in a murine B-cell line and its prevention by bcl-x but not bcl-2. Proc. Natl. Acad. Sci. USA *91*, 7350–7354. https://doi.org/10.1073/pnas.91.15.7350.

43. Muthukkumar, S., Ramesh, T.M., and Bondada, S. (1995). Rapamycin, a potent immunosuppressive drug, causes programmed cell death in B lymphoma cells. Transplantation *60*, 264–270. https://doi.org/10.1097/00007890-199508000-00010.

44. Hammer, Q., Perica, K., van Ooijen, H., Mbofung, R., Momayyezi, P., Varady, E., Martin, K.E., Pan, Y., Jelcic, M., Groff, B., et al. (2023). Genetic ablation of adhesion ligands averts rejection of allogeneic immune cells. Preprint at bioRxiv. 2023.10.09.557143. https://doi.org/10.1101/2023.10.09.557143.

45. Wang, B., Iriguchi, S., Waseda, M., Ueda, N., Ueda, T., Xu, H., Minagawa, A., Ishikawa, A., Yano, H., Ishi, T., et al. (2021). Generation of hypoimmunogenic T cells from genetically engineered allogeneic human induced pluripotent stem cells. Nat. Biomed. Eng. *5*, 429–440. https://doi.org/10.1038/s41551-021-00730-z.

46. Han, X., Wang, M., Duan, S., Franco, P.J., Kenty, J.H.-R., Hedrick, P., Xia, Y., Allen, A., Ferreira, L.M.R., Strominger, J.L., et al. (2019). Generation of hypoimmunogenic human pluripotent stem cells. Proc. Natl. Acad. Sci. USA *116*, 10441–10446. https://doi.org/10.1073/pnas.1902566116.

47. Hu, X., Manner, K., DeJesus, R., White, K., Gattis, C., Ngo, P., Bandoro, C., Tham, E., Chu, E.Y., Young, C., et al. (2023). Hypoimmune anti-CD19 chimeric antigen receptor T cells provide lasting tumor control in fully immunocompetent allogeneic humanized mice. Nat. Commun. *14*, 2020. https://doi.org/10.1038/s41467-023-37785-2.

48. Kosicki, M., Tomberg, K., and Bradley, A. (2018). Repair of double-strand breaks induced by CRISPR-Cas9 leads to large deletions and complex rearrangements. Nat. Biotechnol. *36*, 765–771. https://doi.org/10.1038/nbt.4192.

49. Adikusuma, F., Piltz, S., Corbett, M.A., Turvey, M., McColl, S.R., Helbig, K.J., Beard, M.R., Hughes, J., Pomerantz, R.T., and Thomas, P.Q. (2018). Large deletions induced by Cas9 cleavage. Nature *560*, E8–E9. https://doi.org/10.1038/s41586-018-0380-z.

50. Leibowitz, M.L., Papathanasiou, S., Doerfler, P.A., Blaine, L.J., Sun, L., Yao, Y., Zhang, C.-Z., Weiss, M.J., and Pellman, D. (2021). Chromothripsis as an on-target consequence of CRISPR-Cas9 genome editing. Nat. Genet. *53*, 895–905. https://doi.org/10.1038/s41588-021-00838-7.

51. Sweeney, N.P., and Vink, C.A. (2021). The impact of lentiviral vector genome size and producer cell genomic to gag-pol mRNA ratios on packaging efficiency and titre. Mol. Ther. Methods Clin. Dev. *21*, 574–584. https://doi.org/10.1016/j.omtm.2021.04.007.

52. Grieger, J.C., and Samulski, R.J. (2005). Packaging capacity of adeno-associated virus serotypes: impact of larger genomes on infectivity and postentry steps. J. Virol. *79*, 9933–9944. https://doi.org/10.1128/JVI.79.15.9933-9944.2005.

53. Hess, G., Herbrecht, R., Romaguera, J., Verhoef, G., Crump, M., Gisselbrecht, C., Laurell, A., Offner, F., Strahs, A., Berkenblit, A., et al. (2009). Phase III study to evaluate temsirolimus compared with investigator's choice therapy for the treatment of relapsed or refractory mantle cell lymphoma. J. Clin. Oncol. *27*, 3822–3829. https://doi.org/10.1200/JCO.2008.20.7977.

54. Witzig, T.E., Reeder, C.B., LaPlant, B.R., Gupta, M., Johnston, P.B., Micallef, I.N., Porrata, L.F., Ansell, S.M., Colgan, J.P., Jacobsen, E.D., et al. (2011). A phase II trial of the oral mTOR inhibitor everolimus in relapsed aggressive lymphoma. Leukemia *25*, 341–347. https://doi.org/10.1038/leu.2010.226.

55. Cappell, K.M., and Kochenderfer, J.N. (2023). Long-term outcomes following CAR T cell therapy: what we know so far. Nat. Rev. Clin. Oncol. *20*, 359–371. https://doi.org/10.1038/s41571-023-00754-1.

56. Galli, E., Fresa, A., Bellesi, S., Metafuni, E., Maiolo, E., Pansini, I., Frioni, F., Autore, F., Limongiello, M.A., Innocenti, I., et al. (2024). Hematopoiesis and immune reconstitution after CD19 directed chimeric antigen receptor T-cells (CAR-T): A comprehensive review on incidence, risk factors and current management. Eur. J. Haematol. *112*, 184–196. https://doi.org/10.1111/ejh.14052.

57. Shah, B.D., Ghobadi, A., Oluwole, O.O., Logan, A.C., Boissel, N., Cassaday, R.D., Leguay, T., Bishop, M.R., Topp, M.S., Tzachanis, D., et al. (2021). KTE-X19 for relapsed or refractory adult B-cell acute lymphoblastic leukaemia: phase 2 results of the single-arm, open-label, multicentre ZUMA-3 study. Lancet *398*, 491–502. https://doi.org/10.1016/S0140-6736(21)01222-8.

58. Munshi, N.C., Anderson, L.D., Shah, N., Madduri, D., Berdeja, J., Lonial, S., Raje, N., Lin, Y., Siegel, D., Oriol, A., et al. (2021). Idecabtagene Vicleucel in Relapsed and Refractory Multiple Myeloma. N. Engl. J. Med. *384*, 705–716. https://doi.org/10.1056/NEJMoa2024850.

59. Mackensen, A., Müller, F., Mougiakakos, D., Böltz, S., Wilhelm, A., Aigner, M., Völkl, S., Simon, D., Kleyer, A., Munoz, L., et al. (2022). Anti-CD19 CAR T cell therapy for refractory systemic lupus erythematosus. Nat. Med. *28*, 2124–2132. https://doi.org/10.1038/s41591-022-02017-5.

60. Korell, F., Schubert, M.-L., Sauer, T., Schmitt, A., Derigs, P., Weber, T.F., Schnitzler, P., Müller-Tidow, C., Dreger, P., and Schmitt, M. (2021). Infection Complications after Lymphodepletion and Dosing of Chimeric Antigen Receptor T (CAR-T) Cell Therapy in Patients with Relapsed/Refractory Acute Lymphoblastic Leukemia or B Cell Non-Hodgkin Lymphoma. Cancers (Basel) *13*, 1684. https://doi.org/10.3390/cancers13071684.

61. Avanzi, M.P., Yeku, O., Li, X., Wijewarnasuriya, D.P., van Leeuwen, D.G., Cheung, K., Park, H., Purdon, T.J., Daniyan, A.F., Spitzer, M.H., and Brentjens, R.J. (2018). Engineered Tumor-Targeted T Cells Mediate Enhanced Anti-Tumor Efficacy Both Directly and through Activation of the Endogenous Immune System. Cell Rep. *23*, 2130–2141. https://doi.org/10.1016/j.celrep.2018.04.051.

62. Alizadeh, D., Wong, R.A., Gholamin, S., Maker, M., Aftabizadeh, M., Yang, X., Pecoraro, J.R., Jeppson, J.D., Wang, D., Aguilar, B., et al. (2021). IFNγ Is Critical for CAR T Cell-Mediated Myeloid Activation and Induction of Endogenous Immunity. Cancer Discov. *11*, 2248–2265. https://doi.org/10.1158/2159-8290.CD-20-1661.

63. Xu, L., and Cai, M. (2023). Tacrolimus Maintains the Balance of Neutrophil Extracellular Traps by Inducing DNA Methylation of Neutrophils to Reduce Immune Rejection. Life (Basel) *13*, 2253. https://doi.org/10.3390/life13122253.

64. Kannegieter, N.M., Hesselink, D.A., Dieterich, M., Kraaijeveld, R., Rowshani, A.T., Leenen, P.J.M., and Baan, C.C. (2017). The Effect of Tacrolimus and Mycophenolic Acid on CD14+ Monocyte Activation and Function. PLoS One *12*, e0170806. https://doi.org/10.1371/journal.pone.0170806.

65. Liu, B., Jiang, Q., Chen, R., Gao, S., Xia, Q., Zhu, J., Zhang, F., Shao, C., Liu, X., Li, X., et al. (2022). Tacrolimus ameliorates bleomycin-induced pulmonary fibrosis by inhibiting M2 macrophage polarization via JAK2/STAT3 signaling. Int. Immunopharmacol. *113*, 109424. https://doi.org/10.1016/j.intimp.2022.109424.

66. Gallon, L., Traitanon, O., Yu, Y., Shi, B., Leventhal, J.R., Miller, J., Mas, V., L, X., and Mathew, J.M. (2015). Differential Effects of Calcineurin and Mammalian Target of Rapamycin Inhibitors on Alloreactive Th1, Th17, and Regulatory T Cells. Transplantation *99*, 1774–1784. https://doi.org/10.1097/TP.0000000000000717.

67. Miroux, C., Morales, O., Ghazal, K., Othman, S.B., de Launoit, Y., Pancré, V., Conti, F., and Delhem, N. (2012). In vitro effects of cyclosporine A and tacrolimus on regulatory T-cell proliferation and function. Transplantation *94*, 123–131. https://doi.org/10.1097/TP.0b013e3182590d8f.

68. Furukawa, A., Wisel, S.A., and Tang, Q. (2016). Impact of Immune-Modulatory Drugs on Regulatory T Cell. Transplantation *100*, 2288–2300. https://doi.org/10.1097/TP.0000000000001379.

69. Hudes, G., Carducci, M., Tomczak, P., Dutcher, J., Figlin, R., Kapoor, A., Staroslawska, E., Sosman, J., McDermott, D., Bodrogi, I., et al. (2007). Temsirolimus, interferon alfa, or both for advanced renal-cell carcinoma. N. Engl. J. Med. *356*, 2271–2281. https://doi.org/10.1056/NEJMoa066838.

70. Faes, S., Demartines, N., and Dormond, O. (2021). Mechanistic Target of Rapamycin Inhibitors in Renal Cell Carcinoma: Potential, Limitations, and Perspectives. Front. Cell Dev. Biol. *9*, 636037. https://doi.org/10.3389/fcell.2021.636037.

71. Brown, C.E., Rodriguez, A., Palmer, J., Ostberg, J.R., Naranjo, A., Wagner, J.R., Aguilar, B., Starr, R., Weng, L., Synold, T.W., et al. (2022). Off-the-shelf, steroid-resistant, IL13Rα2-specific CAR T cells for treatment of glioblastoma. Neuro. Oncol. *24*, 1318–1330. https://doi.org/10.1093/neuonc/noac024.

72. Amini, L., Wagner, D.L., Rössler, U., Zarrinrad, G., Wagner, L.F., Vollmer, T., Wendering, D.J., Kornak, U., Volk, H.-D., Reinke, P., and Schmueck-Henneresse, M. (2021). CRISPR-Cas9-Edited Tacrolimus-Resistant Antiviral T Cells for Advanced Adoptive Immunotherapy in Transplant Recipients. Mol. Ther. *29*, 32–46. https://doi.org/10.1016/j.ymthe.2020.09.011.

73. Zhang, Y., Fang, H., Wang, G., Yuan, G., Dong, R., Luo, J., Lyu, Y., Wang, Y., Li, P., Zhou, C., et al. (2023). Cyclosporine A-resistant CAR-T cells mediate antitumour immunity in the presence of allogeneic cells. Nat. Commun. *14*, 8491. https://doi.org/10.1038/s41467-023-44176-0.

74. Jonnalagadda, M., Brown, C.E., Chang, W.C., Ostberg, J.R., Forman, S.J., and Jensen, M.C. (2013). Efficient selection of genetically modified human T cells using methotrexate-resistant human dihydrofolate reductase. Gene Ther. *20*, 853–860. https://doi.org/10.1038/gt.2012.97.

75. Fraietta, J.A., Nobles, C.L., Sammons, M.A., Lundh, S., Carty, S.A., Reich, T.J., Cogdill, A.P., Morrissette, J.J.D., DeNizio, J.E., Reddy, S., et al. (2018). Disruption of TET2 promotes the therapeutic efficacy of CD19-targeted T cells. Nature *558*, 307–312. https://doi.org/10.1038/s41586-018-0178-z.

76. Shah, N.N., Qin, H., Yates, B., Su, L., Shalabi, H., Raffeld, M., Ahlman, M.A., Stetler-Stevenson, M., Yuan, C., Guo, S., et al. (2019). Clonal expansion of CAR T cells harboring lentivector integration in the CBL gene following anti-CD22 CAR T-cell therapy. Blood Adv. *3*, 2317–2322. https://doi.org/10.1182/bloodadvances.2019000219.

77. Brainard, D.M., Seung, E., Frahm, N., Cariappa, A., Bailey, C.C., Hart, W.K., Shin, H.-S., Brooks, S.F., Knight, H.L., Eichbaum, Q., et al. (2009). Induction of robust cellular and humoral virus-specific adaptive immune responses in human immunodeficiency virus-infected humanized BLT mice. J. Virol. *83*, 7305–7321. https://doi.org/10.1128/JVI.02207-08.

78. Leibman, R.S., Richardson, M.W., Ellebrecht, C.T., Maldini, C.R., Glover, J.A., Secreto, A.J., Kulikovskaya, I., Lacey, S.F., Akkina, S.R., Yi, Y., et al. (2017). Supraphysiologic control over HIV-1 replication mediated by CD8 T cells expressing a re-engineered CD4-based chimeric antigen receptor. Plos Pathog. *13*, e1006613. https://doi.org/10.1371/journal.ppat.1006613.

79. Maldini, C.R., Claiborne, D.T., Okawa, K., Chen, T., Dopkin, D.L., Shan, X., Power, K.A., Trifonova, R.T., Krupp, K., Phelps, M., et al. (2020). Dual CD4-based CAR T cells with distinct costimulatory domains mitigate HIV pathogenesis in vivo. Nat. Med. *26*, 1776–1787. https://doi.org/10.1038/s41591-020-1039-5.

80. Nicholson, I.C., Lenton, K.A., Little, D.J., Decorso, T., Lee, F.T., Scott, A.M., Zola, H., and Hohmann, A.W. (1997). Construction and characterisation of a functional CD19 specific single chain Fv fragment for immunotherapy of B lineage leukaemia and lymphoma. Mol. Immunol. *34*, 1157–1165. https://doi.org/10.1016/s0161-5890(97)00144-2.

81. Diorio, C., Murray, R., Naniong, M., Barrera, L., Camblin, A., Chukinas, J., Coholan, L., Edwards, A., Fuller, T., Gonzales, C., et al. (2022). Cytosine base editing enables quadruple-edited allogeneic CART cells for T-ALL. Blood *140*, 619–629. https://doi.org/10.1182/blood.2022015825.

82. Gaudelli, N.M., Lam, D.K., Rees, H.A., Solá-Esteves, N.M., Barrera, L.A., Born, D.A., Edwards, A., Gehrke, J.M., Lee, S.-J., Liquori, A.J., et al. (2020). Directed evolution of adenine base editors with increased activity and therapeutic application. Nat. Biotechnol. *38*, 892–900. https://doi.org/10.1038/s41587-020-0491-6.

83. Hermans, I.F., Silk, J.D., Yang, J., Palmowski, M.J., Gileadi, U., McCarthy, C., Salio, M., Ronchese, F., and Cerundolo, V. (2004). The VITAL assay: a versatile fluorometric technique for assessing CTL- and NKT-mediated cytotoxicity against multiple targets in vitro and in vivo. J. Immunol. Methods *285*, 25–40. https://doi.org/10.1016/j.jim.2003.10.017.

YMTHE, Volume *32*

Supplemental Information

Immunosuppressant therapy averts rejection of allogeneic *FKBP1A*-disrupted CAR-T cells

Colby R. Maldini, Angelica C. Messana, Paula B. Bendet, Adam J. Camblin, Faith M. Musenge, Moriah L. White, Joseph J. Rocha, Lindsey J. Coholan, Cisem Karaca, Frederick Li, Bo Yan, Vladimir D. Vrbanac, Emily Marte, Daniel T. Claiborne, Christian L. Boutwell, and Todd M. Allen

Figure S1

A

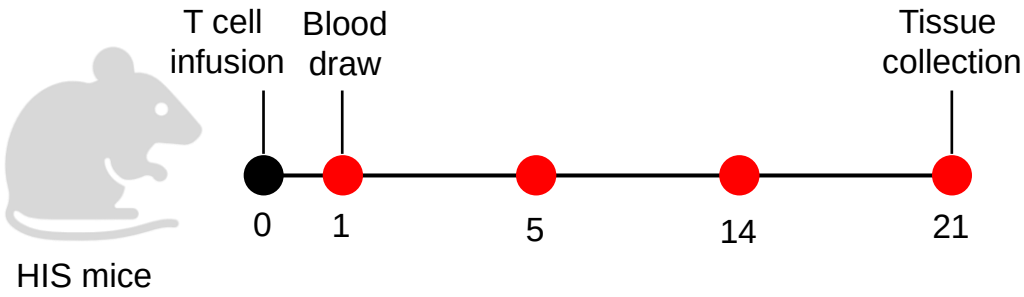

	HLA-I					
T cell donor	A_1	A_2	B_1	B_2	C_1	C_2
Syngeneic	02:01	30:02	18:01	45:01	05:01	16:01
Allogeneic	01:01	31:01	08:01	15:17	07:01	07:01

B

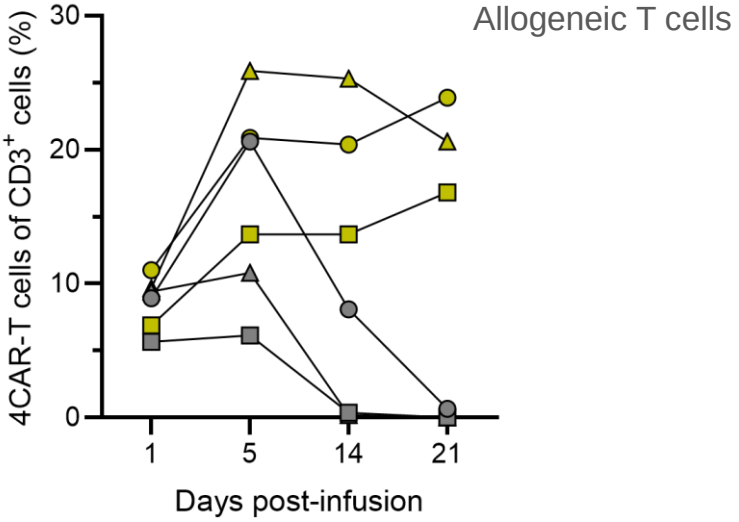

C

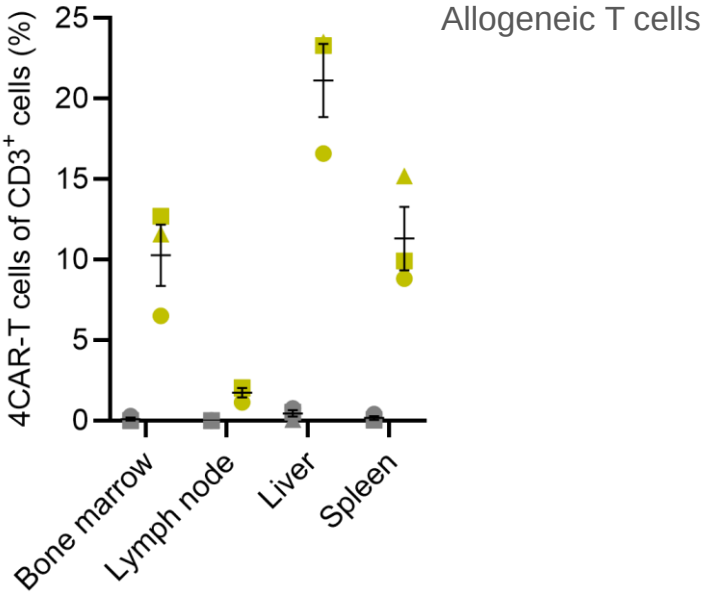

HIS mice reject HLA-mismatched 4CAR-T cells. A Human immune system (HIS) mice (BLT-NSG; n = 3) were infused with 5 x 10^6 CD4-based CAR-T cells (4CAR) of each type derived from a syngeneic HIS mouse donor and an allogeneic HLA-mismatched human donor. **B,C** Longitudinal frequency of 4CAR-T cells in circulation (**B**) and in resected tissues at 3-weeks post-infusion (**C**)**.** For all data, symbols represent individual mice, lines indicate mean and error bars show ±s.e.m.

Figure S2

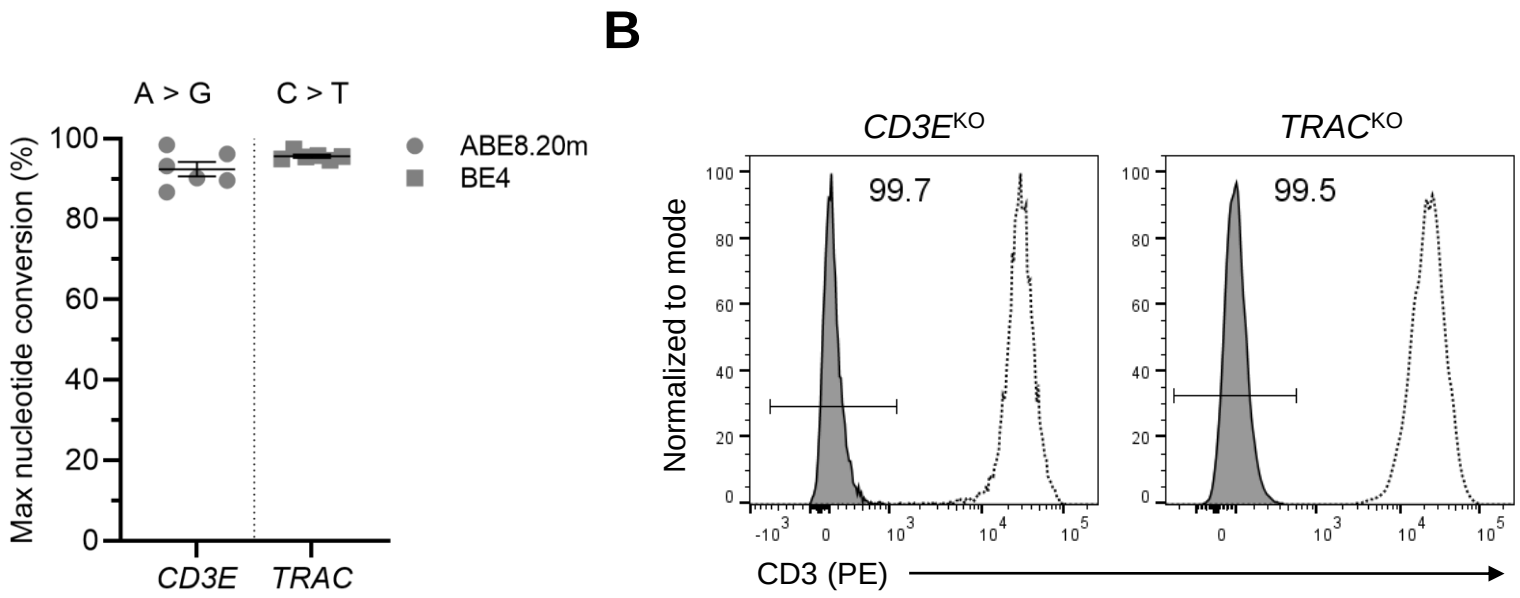

Disruption of *CD3E and TRAC* abrogates T cell receptor surface expression. Human T cells were electroporated with a *CD3E*- or *TRAC*-specific sgRNA complexed with mRNA encoding ABE8.20m or BE4, respectively. **A** Frequency of nucleotide conversion determined by next-generation sequencing in T cells 5-days post-electroporation. Symbols are independent donors. Lines represent mean and error bars show ±s.e.m. **B** Histograms indicate CD3 protein surface expression in base-edited (gray) and unmodified (white) T cells.

Figure S3

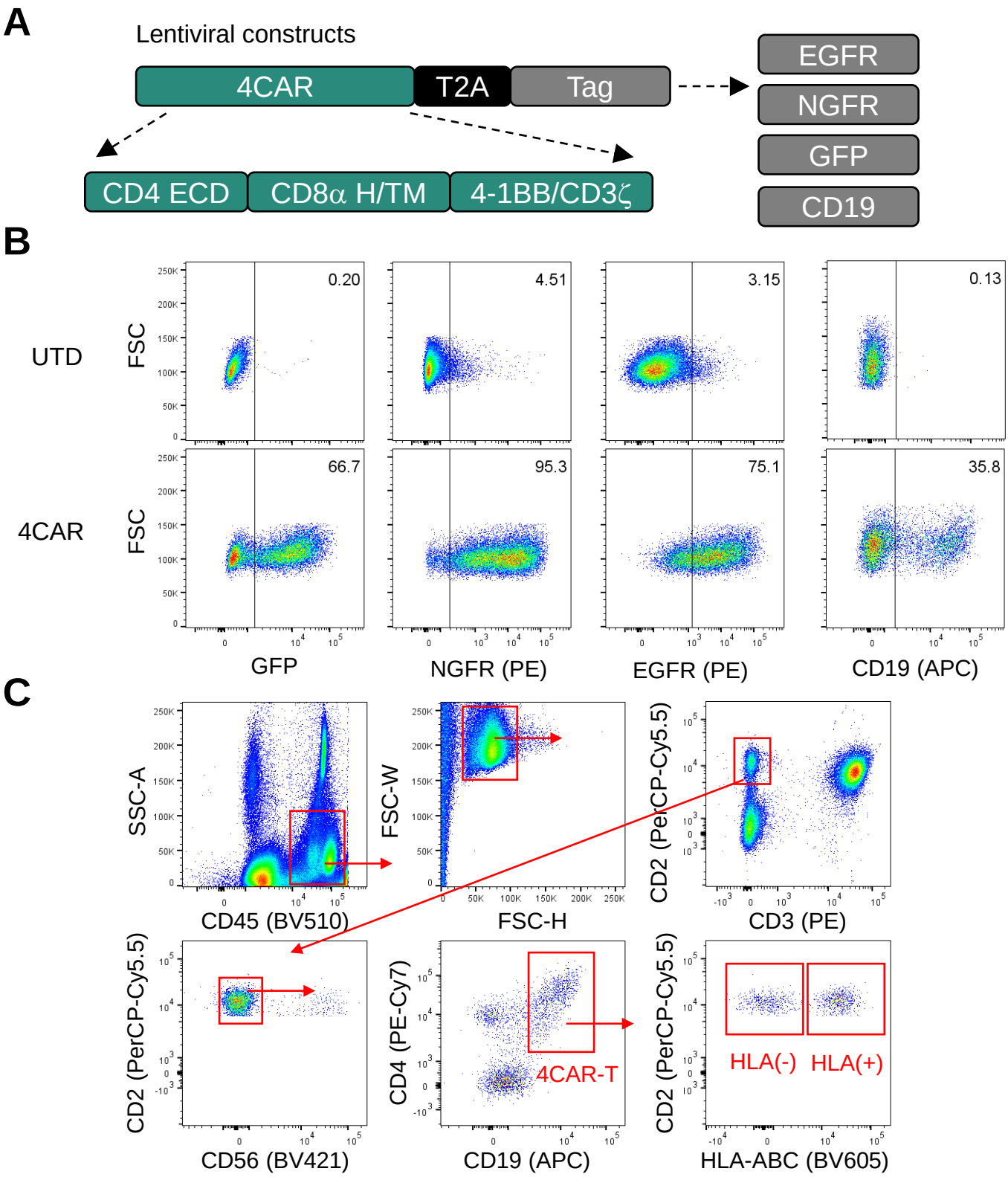

CD4-based CAR-T cell generation and *ex vivo* identification by flow cytometry. A Schematic of lentiviral constructs used to generate CD4-based CAR-T cells. CD4-based CAR (4CAR) consists of the CD4 extracellular domain (ECD) fused to the CD8α hinge (H) and transmembrane (TM) regions along with the intracellular 4-1BB and CD3ζ activating motifs. 4CAR was separated by an intervening T2A self-cleaving peptide to a molecular tag comprising GFP or truncated EGFR, NGFR or CD19. **B** FACS plots indicate frequency of transduced 4CAR-T cells expressing the indicated molecular tag incorporated into the 4CAR lentiviral construct. Untransduced (UTD) T cells were used as a negative control. **C** Representative flow cytometry gating strategy to identify HLA^{+} and HLA-deficient 4CAR-T cells from whole blood or tissue of HIS mice.

Figure S4

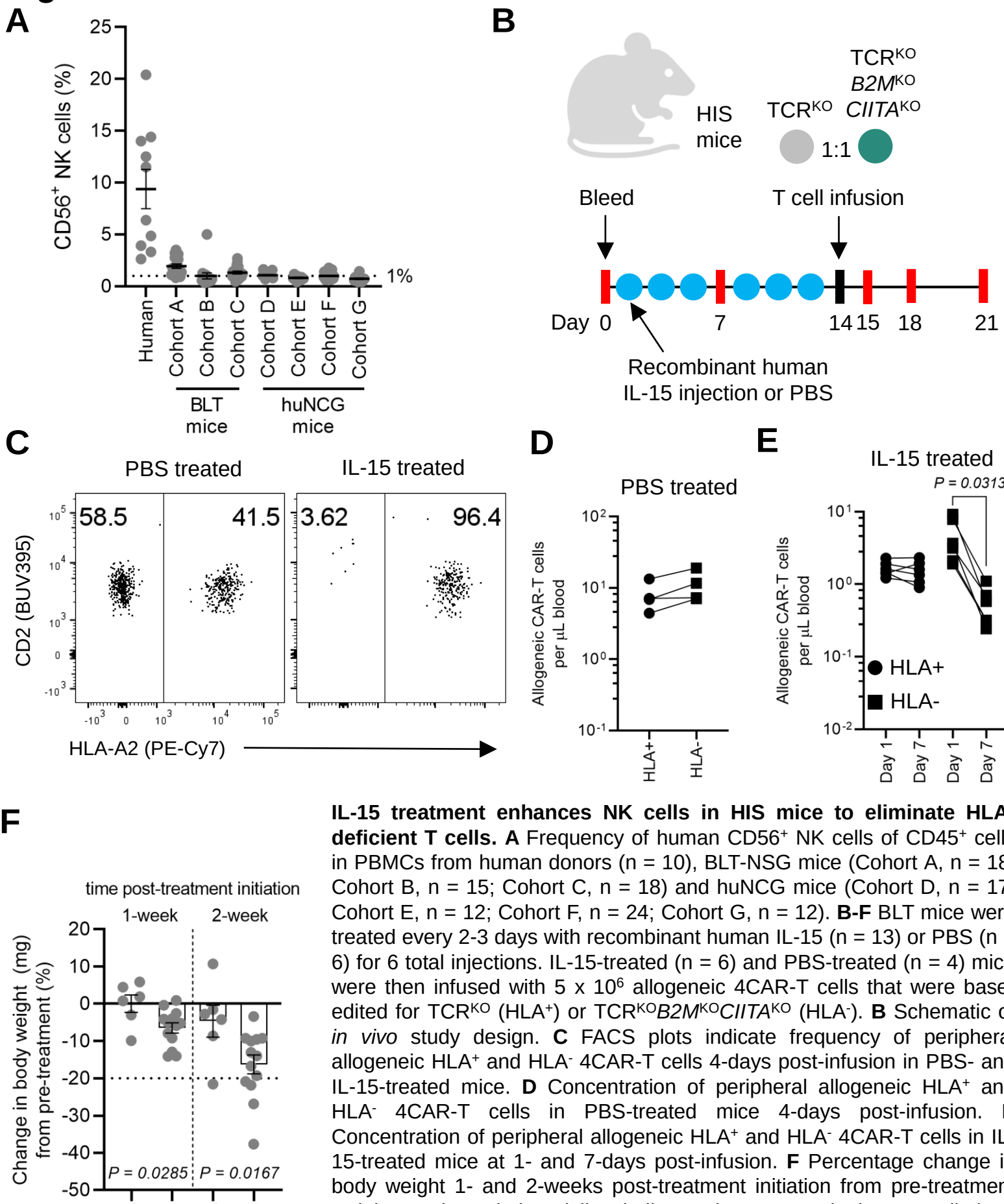

IL-15 treatment enhances NK cells in HIS mice to eliminate HLA-deficient T cells. A Frequency of human CD56$^+$ NK cells of CD45$^+$ cells in PBMCs from human donors (n = 10), BLT-NSG mice (Cohort A, n = 18; Cohort B, n = 15; Cohort C, n = 18) and huNCG mice (Cohort D, n = 17; Cohort E, n = 12; Cohort F, n = 24; Cohort G, n = 12). **B-F** BLT mice were treated every 2-3 days with recombinant human IL-15 (n = 13) or PBS (n = 6) for 6 total injections. IL-15-treated (n = 6) and PBS-treated (n = 4) mice were then infused with 5 x 10^6 allogeneic 4CAR-T cells that were base-edited for TCR^{KO} (HLA$^+$) or TCR^{KO}*B2M*^{KO}*CIITA*^{KO} (HLA$^-$). **B** Schematic of *in vivo* study design. **C** FACS plots indicate frequency of peripheral allogeneic HLA$^+$ and HLA$^-$ 4CAR-T cells 4-days post-infusion in PBS- and IL-15-treated mice. **D** Concentration of peripheral allogeneic HLA$^+$ and HLA$^-$ 4CAR-T cells in PBS-treated mice 4-days post-infusion. **E** Concentration of peripheral allogeneic HLA$^+$ and HLA$^-$ 4CAR-T cells in IL-15-treated mice at 1- and 7-days post-infusion. **F** Percentage change in body weight 1- and 2-weeks post-treatment initiation from pre-treatment weight. Horizontal dotted line indicates humane endpoint. For all data, symbols indicate biologically independent samples. Statistical significance was calculated by Wilcoxon matched-pairs signed rank test (**E**), and Wilcoxon rank sum test (**F**).

Figure S5

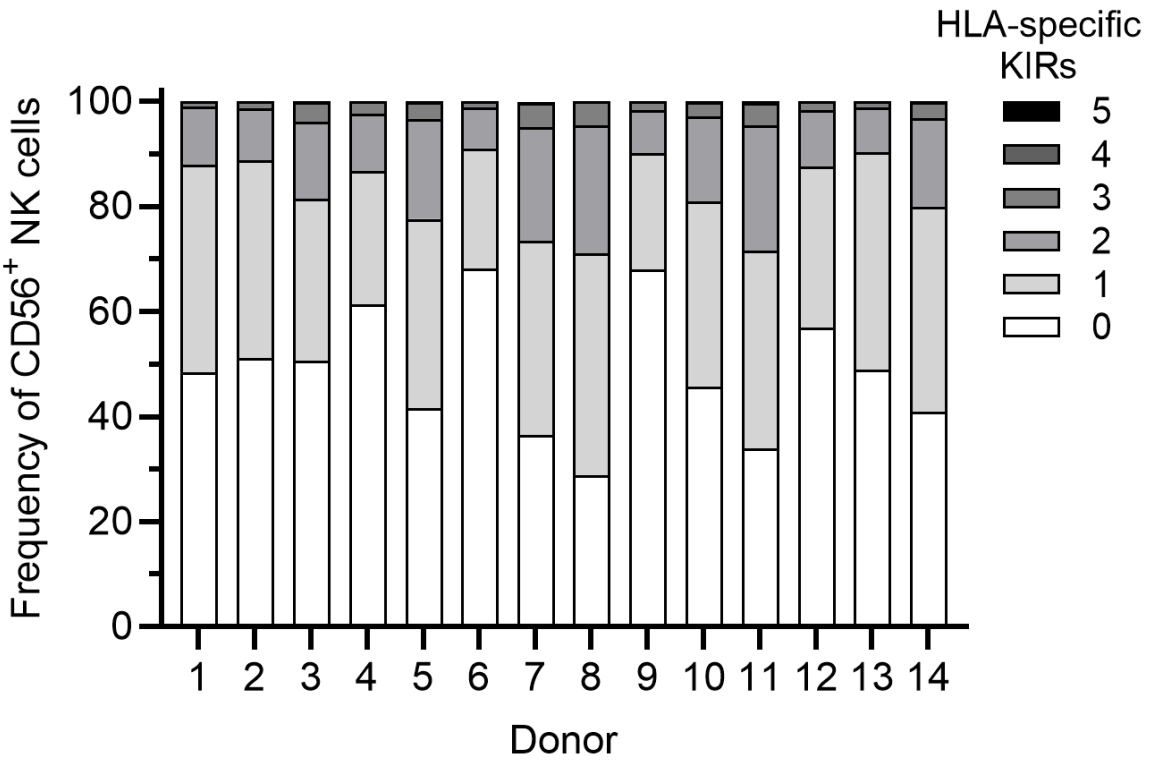

Peripheral blood NK cells express a heterogenous pattern of HLA-specific inhibitory KIRs. Inhibitory KIR expression profile for combinatorial subsets of $CD56^+$ NK cells expressing 0 to 5 KIRs, including KIR2DL1, KIR2DL2/L3, KIR3DL1, KIR2DL4 and KIR2DL5. Data represents 14 independent human donors.

Figure S6

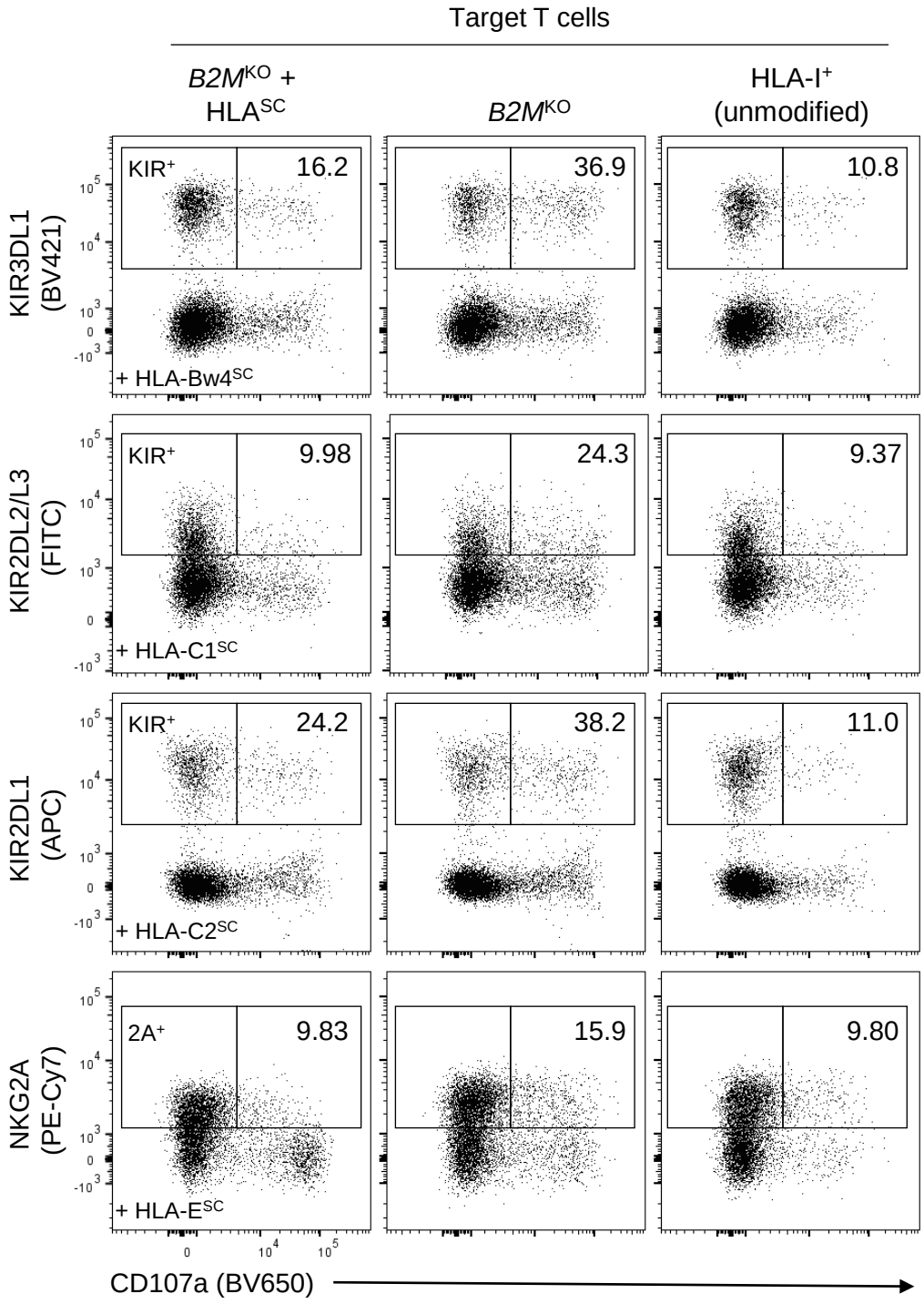

HLA-I deficient T cells expressing an HLA^{SC} molecule inhibit NK cells expressing the corresponding inhibitory receptor. NK cells were stimulated with allogeneic HLA-I^{+} (unmodified) T cells, *B2M*^{KO} T cells, or *B2M*^{KO} T cells engineered to express one HLA^{SC}, either HLA-Bw4^{SC} (HLA-B*57), HLA-C1^{SC} (HLA-C*07:02), HLA-C2^{SC} (HLA-C*04:01), or HLA-E^{SC} (HLA-E*01:03). FACS plots indicate frequency of CD107a^{+} KIRx^{+} or NKG2A^{+} NK cells after stimulation with unmodified T cells, *B2M*^{KO} T cells, or *B2M*^{KO} T cells expressing the HLA^{SC} inhibitory ligand for the corresponding NK cell subset (*i.e.* KIR3DL1-HLA-Bw4^{SC}, KIR2DL2/L3-HLA-C1^{SC}, KIR2DL1-HLA-C2^{SC}, NKG2A-HLA-E^{SC}).

Figure S7

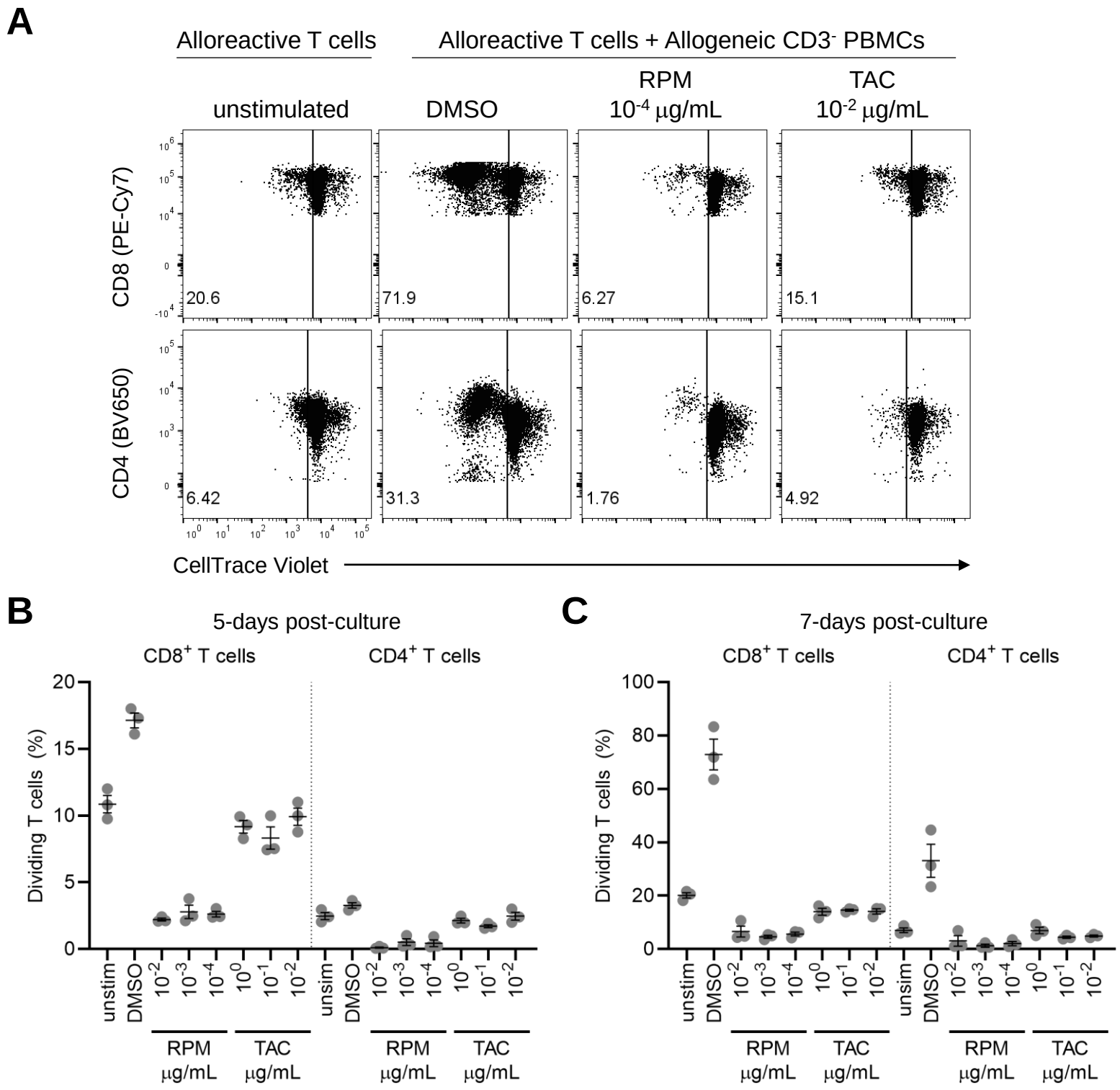

Rapamycin and tacrolimus inhibit *in vitro* priming of alloreactive T cells. Human CD3-depleted PBMCs served as allogeneic target cells to prime CellTrace Violet labeled $CD3^+$ T cells from an HLA-mismatched donor. $CD3^+$ T cells were cultured alone (unstimulated) or in the presence of allogeneic $CD3^-$ PBMCs with DMSO (vehicle), rapamycin (RPM) or tacrolimus (TAC) at different drug concentrations. **A** FACS plots indicate frequency of dividing alloreactive $CD8^+$ and $CD4^+$ T cells 7-days post-culture. **B,C** Frequency of dividing alloreactive $CD8^+$ and $CD4^+$ T cells at 5-days (**B**) and 7-days (**C**) post-culture. Symbols represent independent replicates, lines indicate mean and error bars show ±s.e.m.

Figure S8

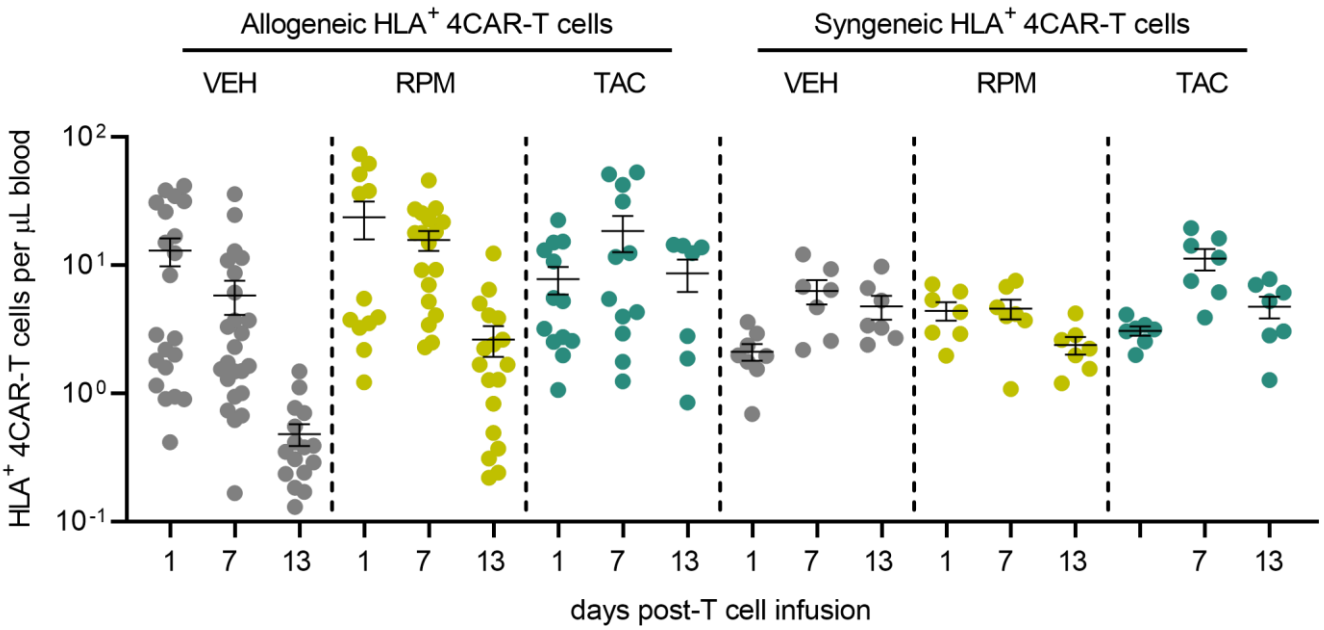

Engraftment of HLA⁺ 4CAR-T cells during drug-treatment interval. Peripheral HLA⁺ 4CAR-T cell concentration in vehicle (VEH), rapamycin (RPM) and tacrolimus (TAC) treated mice measured at 1- and 7- and 13-days post-T cell infusion. Data from allogeneic HLA⁺ 4CAR-T cells represents mice in Cohorts #1 – Cohort #5. Data from syngeneic HLA⁺ 4CAR-T cells represents mice in Cohort #3 and Cohort #4. Symbols represent individual mice, lines indicate mean and error bars show ±s.e.m.

Figure S9

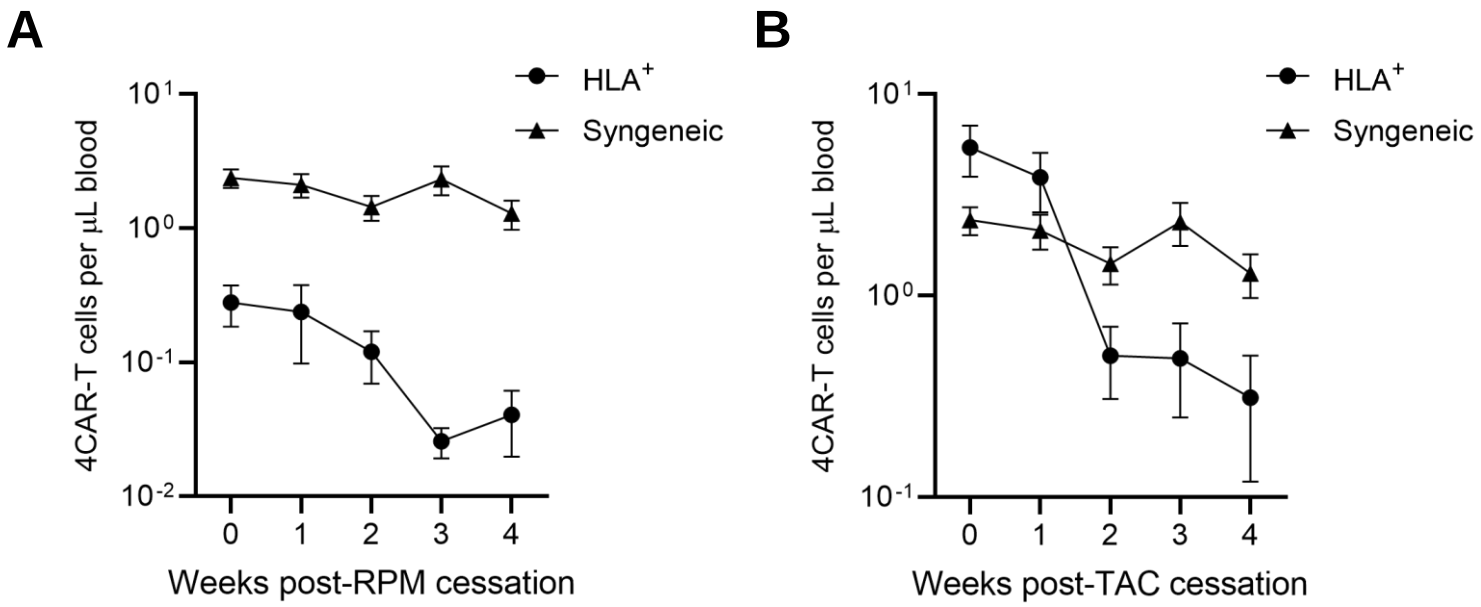

Peripheral allogeneic HLA⁺ 4CAR-T cells are eliminated post-drug treatment withdrawal. huNCG mice from Cohort #3 (n = 4) and Cohort #4 (n = 3) were treated with rapamycin (RPM) or tacrolimus (TAC) daily for 2-weeks. At 1-day post-treatment, 5 x 10^6 allogeneic 4CAR-T cells base-edited for TCR^{KO} (HLA^+) and TCR^{KO}*B2M*^{KO}*CIITA*^{KO} were mixed with 5 x 10^6 syngeneic huNCG mouse-derived 4CAR-T cells and infused into recipient mice. **A,B** Peripheral concentration of allogeneic HLA^+ 4CAR-T cells (circle) and syngeneic 4CAR-T cells (triangle) following RPM (**A**) and TAC (**B**) treatment cessation. Symbols represent mean and errors bars indicate ±s.e.m.

Figure S10

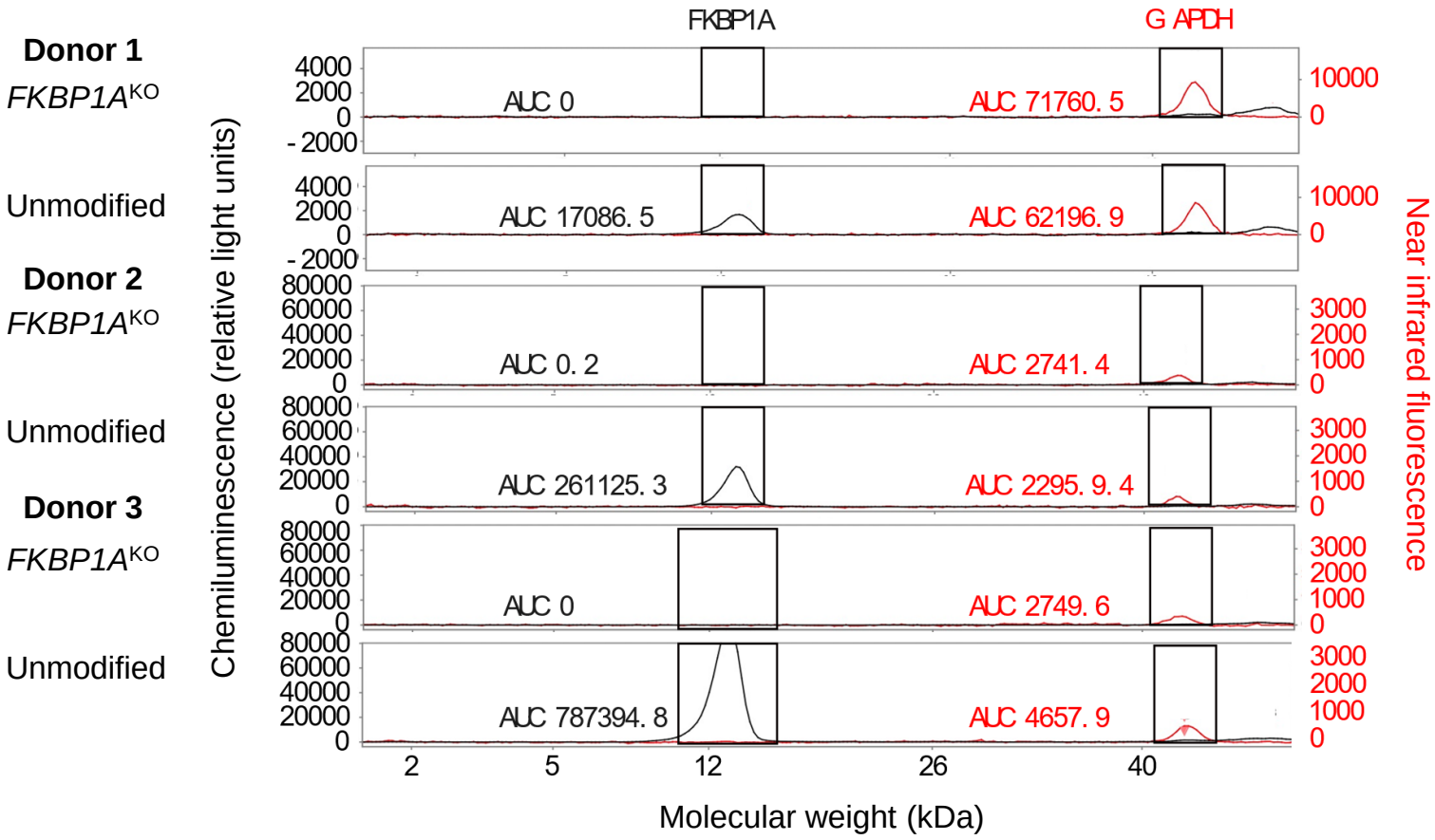

Genetic disruption of *FKBP1A* reduces protein expression. FKBP1A and GAPDH protein detection in unmodified and *FKBP1A*^{KO} T cell lysates from 3 independent donors. Histogram peaks indicate total protein signal from FKBP1A (approximately 12kDa) measured by chemiluminescent fluorescence and GAPDH (approximately 39 kDa) measured by near infrared fluorescence. AUC represents area under the curve of integrated protein signal measured over the indicated ranges (black boxes).

Figure S11

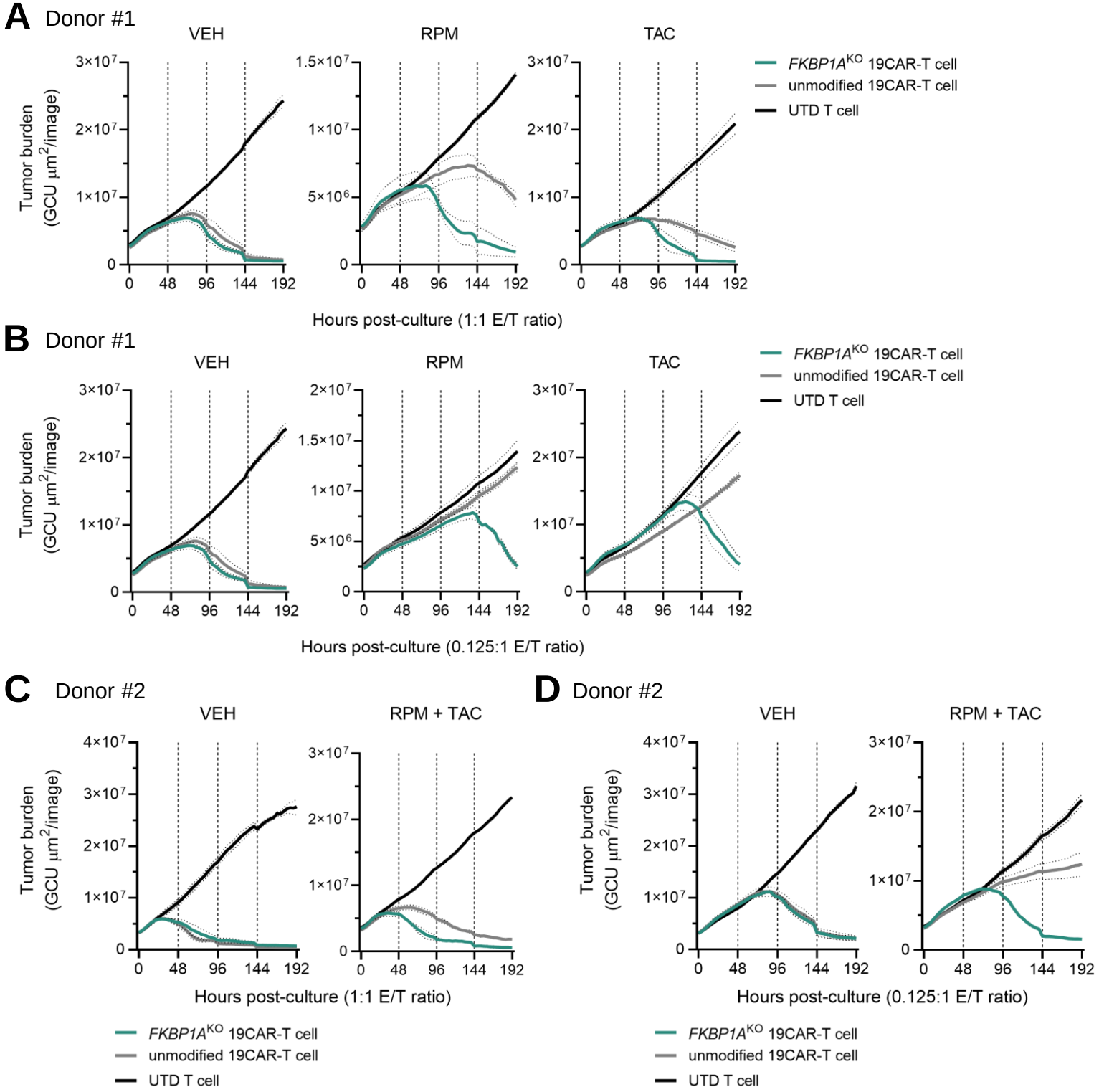

***FKBP1A*^{KO} 19CAR-T cells exhibit *in vitro* anti-tumor cytolytic activity in the presence of rapamycin and tacrolimus.** Incucyte cytotoxicity assay as described in Methods. Tumor burden quantified as Green Calibrated Units (GCU) derived from the fluorescence intensity of GFP^{+} JeKo-1 tumors (targets) cultured in triplicate with effector cells either untransduced (UTD) T cells, unmodified 19CAR-T cells, or *FKBP1A*^{KO} 19CAR-T cells. **A,B** Longitudinal tumor burden at 1:1 (**A**) and 0.125:1 (**B**) effector-to-target (E/T) ratios treated with DMSO vehicle (VEH) control, rapamycin (RPM) or tacrolimus (TAC). **C,D** Longitudinal tumor burden at 1:1 (**C**) and 0.125:1 (**D**) E/T ratios treated with VEH or combination RPM and TAC. Data in **A,B** and **C,D** were generated using independent T cell donors. Bold lines indicate mean GCU from images taken every 4 hours, dotted lines show ±s.e.m., and vertical lines indicate redosing with VEH, RPM and/or TAC.

Figure S12

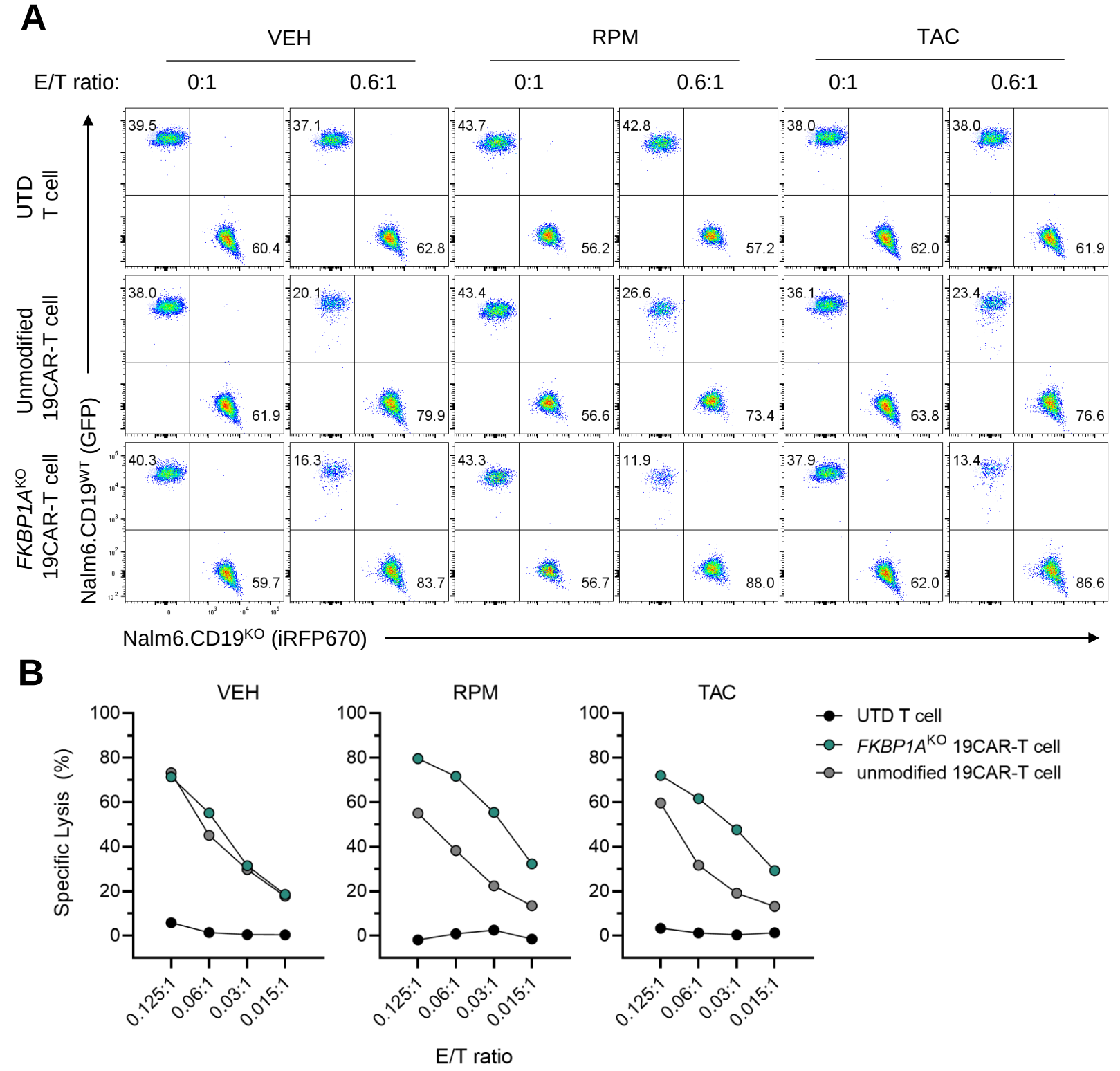

***FKBP1A*^{KO} 19CAR-T cells exhibit *in vitro* anti-tumor cytotoxic activity in the presence of immunosuppressants using VITAL killing assay.** VITAL killing assay as described in Methods. **A** FACS plots indicate frequency of residual on-target Nalm6.CD19^{WT}.GFP^{+} tumor cells and off-target Nalm6.CD19^{KO}.iRFP670^{+} tumor cells at 0:1 and 0.6:1 effector-to-target (E/T) ratio with untransduced (UTD) T cells, unmodified 19CAR-T cells, or *FKBP1A*^{KO} 19CAR-T cells at 48 hours post-culture. Cultures were treated with DMSO vehicle (VEH) control, rapamycin (RPM) or tacrolimus (TAC) at the start of the assay. **B** Summary data indicates frequency of specific lysis at the indicated E/T ratios in VEH-, RPM- and TAC-treated conditions 48 hours post-culture. Symbols represent mean from conditions set-up in duplicate. T cells were generated using an independent donor from Donor #1 and Donor #2 in Figure S11.

Figure S13

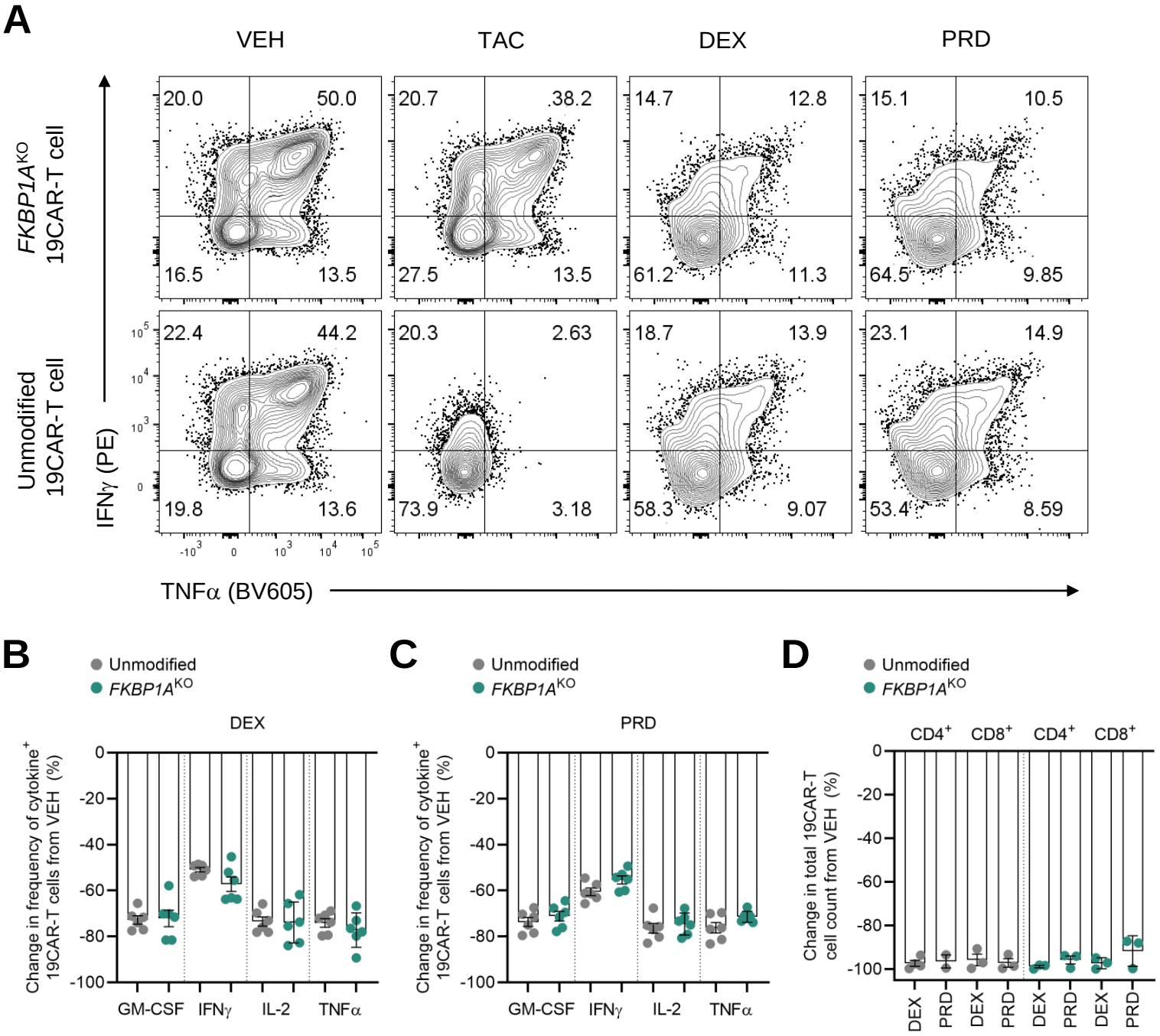

***FKBP1A*^{KO} 19CAR-T cells are sensitive to dexamethasone and prednisone immunosuppression.** Unmodified and *FKBP1A*^{KO} 19CAR-T cells were stimulated with JeKo-1 tumor cells in the presence of DMSO vehicle (VEH) control, tacrolimus (TAC), dexamethasone (DEX) or prednisone (PRD) and then analyzed for intracellular production of cytokines (**A-C**) and proliferation (**D**). FACS plots show frequency of IFNγ and TNFα producing 19CAR-T cells (**A**) and summary data indicates percentage change in frequency of cytokine-positive 19CAR-T cells treated with DEX (**B**) or PRD (**C**) relative to VEH control. Symbols represent 3 independent donors in duplicate. **D** Percentage change in total 19CAR-T cell counts in conditions exposed to DEX or PRD relative to VEH control at 7-days post-stimulation. Symbols represent average of 3 independent donors in triplicate. For all data, bars indicate mean and error bars show ±s.e.m.

Figure S14

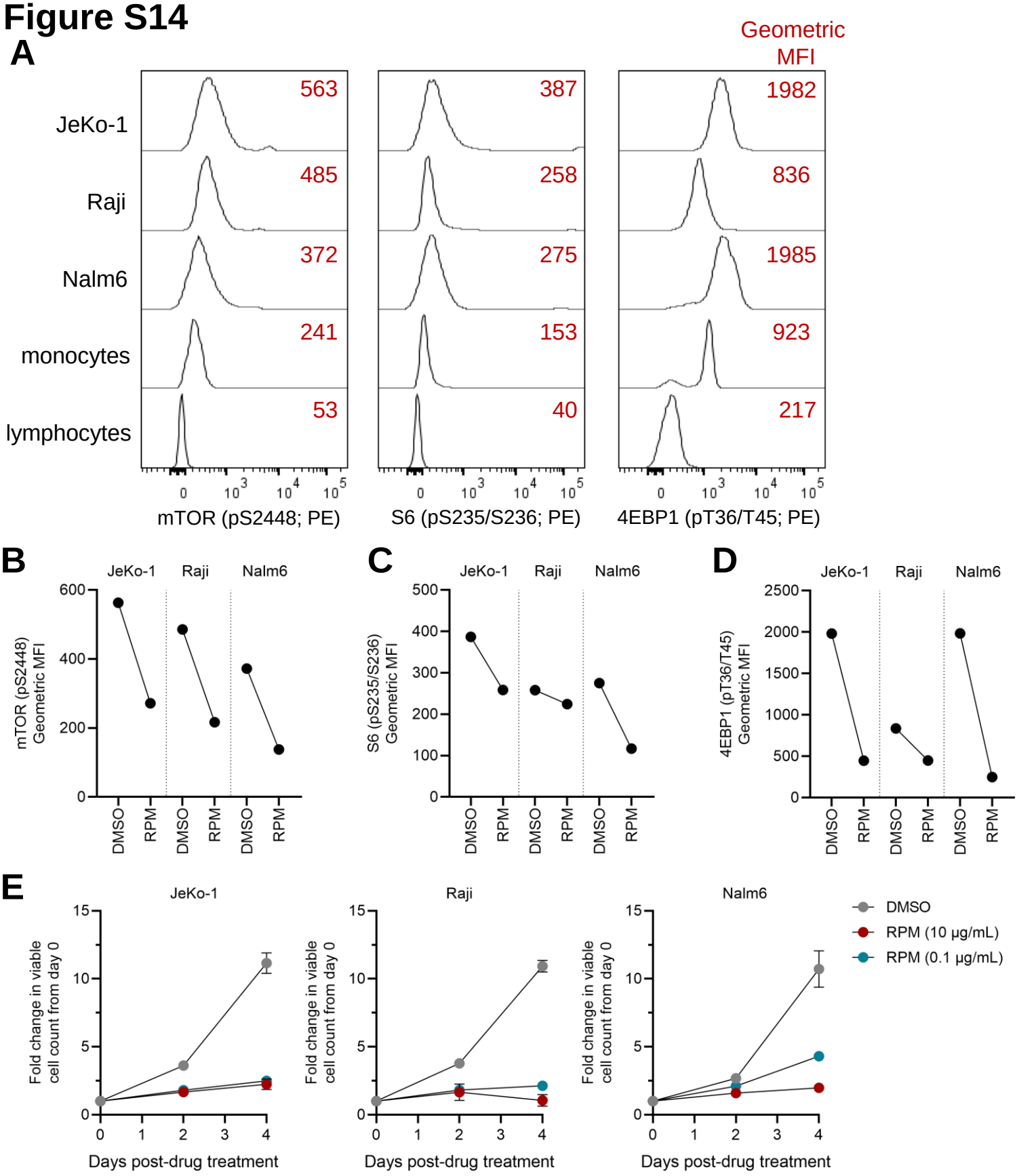

Malignant B cell lines are sensitive to rapamycin treatment *in vitro.* **A** Histograms indicate geometric median fluorescent intensity (MFI) of phosphorylated mTOR (pS2448), S6 (pS235/S2346) and 4EBP1 (pT36/T45) in JeKo-1, Raji and Nalm6 cell lines, as well as primary human monocytes and bulk lymphocytes. **B-D** JeKo-1, Raji and Nalm6 cells were treated with DMSO or rapamycin (RPM) and then analyzed for phosphorylation level of mTOR (**B**), S6 (**C**) and 4EBP1 (**D**). **E** JeKo-1, Raji and Nalm6 cell growth kinetics on 2- and 4-days post-treatment with DMSO or RPM at different drug concentrations. Symbols indicate mean of triplicate samples and error bars show ±s.e.m.

Table S1

Protospacer, base-editor and amplification primers for all target genes

Target Gene	sgRNA ID	Protospacer sequence	Editor (s)	PCR amplification primer (forward)	PCR amplification primer (reverse)
B2M	TSBTx760	CTTACCCCACTTAACTATCT	ABE8.20m	TGTCTTTCAGCAAGGACTGGTCTTTCTA	GACTCATTCAGGGTAGTATGGCCATAGA
B2M	TSBTx845	ACTCACGCTGGATAGCCTCC	rBE4	CGCGCTGGCGGGCATTCCTGAAGCTGA	GCGGGCCACCAAGGAGAACTTGGAGAA
CIITA	TSBTx763	CACTCACCTTAGCCTGAGCA	ABE8.20m / rBE4	ATCACTGACCTGGGTGCCTACAAA	AGAGTTTCTTTCACCACGTCCCGCTAA
CD3E	TSBTx4073	CTGGATTACCTCTTGCCCTC	ABE8.20m	GGATCACCTGTCACTGAAGGAATTTTCA	CGCAAAGACGCCTGGGCACTGTGA
TRAC	TSBTx754	TTCGTATCTGTAAAACCAAG	rBE4	GAGCTGCAGGCCTCCCCCACCCA	GCAGATTAAACCCGGCCACTTTCAGG
FKBP1A	TSBTx1538	CTCACCGTCTCCTGGGGAGA	ABE8.20m	CCGAGGTACTAGGCAGAGC	CCCTGAGGAGACAGAGACGG
FKBP1A	TSBTx1542	ACCGGTGTAGTGCACCACGC	ABE8.20m	CCCAGGAGACGGTGAGTAGT	CCTCGACGGCCAGCC
FKBP1A	TSBTx1545	TACCCAAGAACAGGGAGCTA	ABE8.20m	TATGCCTATGGTGCCACTGG	CTCTGCTACCCATCAAACGC
FKBP1A	TSBTx1546	CCCCAACAGATCTGCCATGG	ABE8.20m	GTCGCCACTGCACACAAAG	TCGGAAGCAAAGCTGAG
FKBP1A	TSBTx1581	TTCACAGGGATGCTTGAAGA	ABE8.20m	TGATGAGTGCTCTGCTGCTG	GAGAGAGCATACCTGGGCAA
FKBP1A	TSBTx1582	CGCCGCCATGGGAGTGCAGG	ABE8.20m	CCGAGGTACTAGGCAGAGC	CCCTGAGGAGACAGAGACGG
FKBP1A	TSBTx1537	CAGGTGGAAACCATCTCCCC	rBE4	CCGAGGTACTAGGCAGAGC	CCCTGAGGAGACAGAGACGG
FKBP1A	TSBTx1538	CTCACCGTCTCCTGGGGAGA	rBE4	CCGAGGTACTAGGCAGAGC	CCCTGAGGAGACAGAGACGG
FKBP1A	TSBTx1539	GCGCCCTGAGGAGACAGAGA	rBE4	CCCAGGAGACGGTGAGTAGT	CCTCGACGGCCAGCC
FKBP1A	TSBTx1540	CGCCCTGAGGAGACAGAGAC	rBE4	CCCAGGAGACGGTGAGTAGT	CCTCGACGGCCAGCC
FKBP1A	TSBTx1541	CAAGCGCGGCCAGACCTGCG	rBE4	CCCAGGAGACGGTGAGTAGT	CCTCGACGGCCAGCC
FKBP1A	TSBTx1542	ACCGGTGTAGTGCACCACGC	rBE4	CCCAGGAGACGGTGAGTAGT	CCTCGACGGCCAGCC
FKBP1A	TSBTx1543	ACTCATCTGTGAAAAGAACA	rBE4	GGCCAAGGAACACCTAGGTA	GAAGCTCCACATCGAAGACG
FKBP1A	TSBTx1544	CGATGTGGAGCTTCTAAAAC	rBE4	TATGCCTATGGTGCCACTGG	CTCTGCTACCCATCAAACGC
FKBP1A	TSBTx1545	TACCCAAGAACAGGGAGCTA	rBE4	TATGCCTATGGTGCCACTGG	CTCTGCTACCCATCAAACGC
FKBP1A	TSBTx1577	AGCAGGAGGTGATCCGAGGC	rBE4	CACAGGGATGCTTGAAGATGG	CACAGGGATGCTTGAAGATGG
FKBP1A	TSBTx1578	GCAGGAGGTGATCCGAGGCT	rBE4	CACAGGGATGCTTGAAGATGG	CACAGGGATGCTTGAAGATGG
FKBP1A	TSBTx1579	GTGATCCGAGGCTGGGAAGA	rBE4	CACAGGGATGCTTGAAGATGG	CACAGGGATGCTTGAAGATGG
FKBP1A	TSBTx1580	GATCCGAGGCTGGGAAGAAG	rBE4	CACAGGGATGCTTGAAGATGG	CACAGGGATGCTTGAAGATGG
CD19	TSBTx3773	CCAGACCTCACCATGGCCCC	ABE8.20m	-	-

Table S2

HLA class-I typing for human allogeneic CAR-T cell donors and HIS mice

Figure	HIS mouse strain	Cohort	HLA class-I typing	Allogeneic T cell donor	HLA class-I typing
1F-H	BLT-NSG	-	A*01:01 A*31:01 B*52:01 B*57:01 C*06:02 C*12:02	DC71	A*02:01 A*24:02 B*17:02 B*15:01 C*03:03 C*05:01
3	BLT-NSG	2	A*68:01:01 A*74:01:01 B*53:01:01 B*58:02:01 C*04:01:01 C*06:02:01	TALL106	A*30*02:01 A*80:01:01 B*18:01:01 B*42:02:01 C*02:02:02 C*17:01:01
3	huNCG	3	A*02:05:01 A*23:17:01 B*15:03:01 B*35:01:01 C*02:10:01 C*04:01:01	D341119	A*01:01:01 A*24:02:01 B*37:01:01 B*39:01:01 C*06:02:01 C*07:02:01
3	huNCG	4	A*01:01:01 A*02:01:01 B*08:01:01 B*35:12:01 C*04:01:01 C*07:01:01	D341119	A*01:01:01 A*24:02:01 B*37:01:01 B*39:01:01 C*06:02:01 C*07:02:01
3	BLT-NSG	5	A*02:01:01 A*23:17:01 B*53:01:01 B*82:02:01 C*04:01:01 C*08:02:01	D341388	A*23:01:01 A*68:01:02 B*44:02:01 B*44:03:01 C*07:04:01 C*07:04:01
6	huNCG	6	A*01:01:01 A*32:01:01 B*08:01:01 B*14:01:01 C*07:01:01 C*08:02:01	CPD-PT060	A*24:02:01 A*68:01:02 B*35:10:00 B*51:01:01 C*03:04:01 C*15:02:01
6	huNCG	7	A*02:01:01 A*02:06:01 B*35:01:01 B*50:02:01 C*06:02:01 C*07:02:01	CPD-PT060	A*24:02:01 A*68:01:02 B*35:10:00 B*51:01:01 C*03:04:01 C*15:02:01
6	huNCG	8	A*02:01:01 A*30:01:01 B*15:01:01 B*38:01:01 C*03:03:01 C*12:03:01	CPD-PT060	A*24:02:01 A*68:01:02 B*35:10:00 B*51:01:01 C*03:04:01 C*15:02:01
6	huNCG	9	A*03:01:01 A*26:01:01 B*27:05:02 B*44:03:01 C*01:02:01 C*16:01:01	CPD-PT060	A*24:02:01 A*68:01:02 B*35:10:00 B*51:01:01 C*03:04:01 C*15:02:01
S1A	BLT-NSG	-	A*02:01 A*30:02 B*18:01 B*45:01 C*05:01 C*16:01	DC70	A*01:01 A*31:01 B*08:01 B*15:17 C*07:01 C*07:01